Title

Midpoint attractors and species richness: Modelling the interaction between environmental drivers and geometric constraints

Journal

Ecology Letters, 19(9)

ISSN

1461-023X

Authors

Colwell, Robert K
Gotelli, Nicholas J
Ashton, Louise A
et al.

Publication Date

2016-09-01

DOI

10.1111/ele.12640

Peer reviewed

Title: **Midpoint attractors and species richness: Modeling the interaction between environmental drivers and geometric constraints**

Short title: Midpoint attractors and species richness

Robert K. Colwell[a,b,c,1], Nicholas J. Gotelli[d], Louise A. Ashton[e,f], Jan Beck[c,g], Gunnar Brehm[h], Tom M. Fayle[i,j,k], Konrad Fiedler[l], Matthew L. Forister[m], Michael Kessler[n], Roger L. Kitching[e], Petr Klimes[i], Jürgen Kluge[o], John T. Longino[p], Sarah C. Maunsell[e], Christy M. McCain[c,q], Jimmy Moses[r,s], Sarah Noben[n], Katerina Sam[i], Legi Sam[e,i], Arthur M. Shapiro[t], Xiangping Wang[u], and Vojtech Novotny[i,r].

[a]Department of Ecology and Evolutionary Biology, University of Connecticut, Storrs, CT 06269, USA

[b]Departmento de Ecologia, Universidade Federal de Goiás, CP 131, 74.001-970, Goiânia, GO, Brasil.

[c]University of Colorado Museum of Natural History, Boulder, CO 80309, USA

[d]Department of Biology, University of Vermont, Burlington, VT 05405, USA

[e]Environmental Futures Research Institute, Griffith University, Nathan, Qld 4111, Australia

[f]Life Sciences Department, Natural History Museum, South Kensington, London SW7 5BD, UK

[g]University of Basel, Department of Environmental Science (Biogeography), Basel, Switzerland

[h]Phyletisches Museum, Friedrich-Schiller Universität, 07743 Jena, Germany

[i]Institute of Entomology, Biology Centre of the Czech Academy of Sciences and Faculty of Science, University of South Bohemia, Branišovská 31, 370 05 České Budějovice, Czech Republic

[j]Forest Ecology and Conservation Group, Imperial College London, Silwood Park Campus, Buckhurst Road, Ascot, Berkshire, SL5 7PY, UK

[k]Institute for Tropical Biology and Conservation, Universiti Malaysia Sabah, 88400 Kota Kinabalu, Sabah, Malaysia

[l]Department of Botany & Biodiversity Research, University of Vienna, Rennweg 14, 1030 Vienna, Austria

[m]Program in Ecology, Evolution, and Conservation Biology, Department of Biology, University of Nevada, Reno, NV 89557, USA

[n]Institute of Systematic Botany, University of Zurich, 8008 Zurich, Switzerland

[o]Department of Geography, University of Marburg, 35032 Marburg, Germany

[p]Department of Biology, University of Utah, Salt Lake City, UT 84112, USA

[q]Department of Ecology and Evolutionary Biology, University of Colorado, Boulder, CO 80309, USA

[r]New Guinea Binatang Research Center, P.O. Box 604, Madang, Papua New Guinea

[s]School of Natural and Physical Sciences, University of Papua New Guinea, P.O. Box 320, National Capital District, Papua New Guinea

[t]Center for Population Biology, University of California, Davis, CA 95616, USA

[u]College of Forestry, Beijing Forestry University, Beijing, 100083, China

[1]To whom correspondence should be addressed. Mailing address: 3572 Smuggler Way, Boulder, CO 80305. Telephone: 1-860-428-5633. Email: robertkcolwell@gmail.com.

Note to Editors and Reviewers:

This pdf file is organized as follows:

1. **Main Text:** Title Page, Abstract, Introduction, Materials And Methods, Results, Discussion, Acknowledgements
2. **References:** A single, integrated list for both the Main Text and Appendices
3. **Appendix 1:** Supplemental Introduction, Materials and Methods, Results, and Discussion
4. **Appendix 2:** Supplemental tables (and supplemental figures, when published)
5. **All Figures with Figure Captions:** Main Text figures and Supplemental Figures together

ABSTRACT:

To model the diverse patterns of species richness patterns on mountainsides, we conjectured that a unimodal gradient of environmental favorability— spanning the elevational domain but not necessarily centered on it— may interact with geometric constraints imposed by sea level and the mountaintop to produce taxon-specific patterns of species richness.. We developed a Bayesian simulation model to estimate the location and strength of such a *midpoint attractor.*. We also constructed *midpoint predictor* models to test whether environmental variables could directly account for the observed patterns of species range midpoints...We challenged these models with 16 elevational datasets, comprising 4500 species of insects, vertebrates, and plants. Whereas the midpoint predictor models generally failed to match the pattern of species midpoints, the midpoint attractor model closely reproduced empirical spatial patterns of species richness and range midpoints.. Gradients of environmental favorability, subject to geometric constraints, may parsimoniously account for elevational patterns of species richness.

Keywords: biogeography | elevational gradients | geometric constraints | mid-domain effect | stochastic model | Bayesian model | truncated niche

INTRODUCTION

Along any continental latitudinal transect, species richness for most higher taxa peaks in the tropics, where mean annual temperature is the highest and annual variability in temperature is lowest (Wright *et al.* 2009). Regardless of latitude, temperature on most mountainsides declines steadily with elevation, driven by adiabatic cooling, so that the warmest temperatures usually prevail at the bottom of elevational gradients (Ahrens 2006; Fan & van den Dool 2008). Net primary productivity (NPP), although crucially dependent on precipitation, is strongly driven by temperature. Thus, if radiant energy or NPP are fundamentally responsible for the latitudinal richness pattern, as many ecologists believe (Currie *et al.* 2004; Allen *et al.* 2007), species richness for higher taxa along elevational transects in humid climates should be expected to peak at the lowest elevations.

However, in a review of hundreds of published examples, Rahbek (1995, 2005) showed that species richness usually does *not* peak at the bottom of elevational gradients. For the preponderance (70%) of studies that encompassed complete elevational gradients and accounted for sampling effects, species richness peaked, instead, at intermediate elevations. Declining richness with elevation was the second most-common pattern, but was found in less than 20% of studies (Rahbek 2005). Among other things, these meta-analyses imply that, for most terrestrial taxa, local species richness peaks at intermediate tropical elevations, rather than in the tropical lowlands

Many explanations have been proposed for mid-elevation richness peaks, and surely no single factor is responsible. For some clades, intermediate climatic conditions at

these elevations may be more suitable for survival and reproduction: lower elevations may be too hot or too dry (McCain 2007) and higher elevations too cold, too wet, or too cloudy (Longino *et al.* 2014). A history of net diversification, together with climatic niche conservatism, can lead to a buildup of species at intermediate elevations (Graham *et al.* 2014; Wu *et al.* 2014). In the tropics, a history of mountaintop extinctions during glacial minima and sea-level extinctions during glacial maxima could also produce or enhance mid-elevation richness peaks (Colwell & Rangel 2010). Spatially structured dispersal within an elevational domain, such as source-sink dynamics (Grytnes 2003; Grytnes *et al.* 2008) or ecotonal mixing (Lomolino 2001), could also lead to peaks of species richness at intermediate elevations.

Geometric constraints. In addition to these ecological and historical explanations, Colwell and Hurtt (1994) showed, with a simple stochastic model, that a mid-elevation richness peak might be expected even in the absence of climatic drivers or historical forces. In their model, a mid-elevation richness peak arises from the tendency of larger species ranges to overlap more at mid-elevations than at high or low elevations, when they are *geometrically constrained* by the hard boundaries (sea level and the mountaintop) of an elevational domain. Fig. 1A offers a physical analogy (a pencil-box) for this phenomenon, which later became known as the *mid-domain effect* (Colwell & Lees 2000) or MDE, because, in a simple 1-dimensional domain, the expected distribution of species richness in this model is exactly symmetrical about the center of the domain. Geometric constraints have been generalized to other bounded spatial (Storch *et al.* 2006) and non-spatial (Letten *et al.* 2013) domains at the assemblage level, as well

as to studies of home ranges (Prevedello *et al.* 2013) and even the movement of individuals within a population (Tiwari *et al.* 2005).

Early studies treated geometric constraints as a stand-alone hypothesis, subject to falsification if it failed to fully explain patterns of richness (Colwell *et al.* 2004, 2005), or strictly as an alternative hypothesis to environmental explanations (Currie & Kerr 2008). But this either/or perspective misses the point that constraints and drivers do not operate independently, but instead interact. It has proven challenging to integrate geometric constraints with environmental and historical explanations for patterns of species richness. We review the history of these efforts in *Appendix 1, Supplemental Introduction*.

A Bayesian midpoint attractor model. Here, we take a novel approach to integrating environment with geometric constraints over elevational gradients. Inspired by Wang and Fang's (2012) evidence that large- and small-ranged species respond similarly to environmental drivers and by Rangel and Diniz-Filho's (2005) mechanistic model, we postulated the presence of an underlying unimodal "favorability" gradient, specific to each elevational transect and to each taxon or functional group.

We modeled the simplest possible pattern of environmental favorability—a unimodal peak—on the simplest possible domain—the unit line. The model is general, but in this study, we assume that the one-dimensional unit domain represents an elevational transect from low elevation (sea level, for all our datasets) to the highest habitable point on a mountain massif. Somewhere along this elevational domain lies a unimodal *midpoint attractor*, specific to the locality and taxon, representing a gradient of attraction for species' range midpoints, a continuous function describing the relative strength of the attractor at every point within the domain (Fig. 1C).

We model the midpoint attractor as a normal (Gaussian) probability density function $N(A, B)$ with two parameters: its mean location A ($0 < A < 1$) on the unit-line domain, and its standard deviation B ($0 < B < 1$) around the attractor, an inverse measure of attractor strength (Fig. 1C). Because the unit domain is bounded at 0 and 1, A and B determine not only the location and shape of the attractor, but also jointly determine where the attractor distribution is truncated by the domain limits. To simulate a bounded elevational richness pattern driven by the midpoint attractor, we place the empirical elevational ranges (transformed to unit-line equivalents) on the domain stochastically, drawing their midpoints from the modeled attractor distribution. Fig. 1B updates the pencil-box analogy for the classic MDE by adding an off-center attractor for pencil midpoints.

We developed a Bayesian model to estimate the optimum shape and position of the midpoint attractor for a particular taxon on a particular elevational gradient.. The model aims to explain the empirical location of species elevational ranges (as indexed by their elevational midpoints), and thus to account for empirical patterns of richness on mountainsides, under geometric constraints. With a centered Gaussian distribution as the starting point (a conjugate prior), the model employs a simple Gibbs sampler to find the parameter values for the attractor (its location, A, and strength, B), that are most probable (P(model | data)), given the observed elevational pattern of species richness and the empirical *range-size frequency distribution* (RSFD) (Gelman *et al.* 2013).

The midpoint attractor model does not incorporate any environmental data into the estimation of these parameters. It makes no assumptions or *a priori* hypotheses about which environmental or biotic factors might be driving the attractor and the favorability

gradient it represents. Instead, once a well-fitting attractor model has been identified using this approach, we subsequently attempt to interpret the attractor statistically in terms of empirically-measured environmental variables.

Whereas the midpoint attractor model maximizes *P*(model | data), most previous attempts to interpret richness patterns have, instead, been conducted in a traditional, frequentist framework, estimating the probability of the data (observed richness), given a specified multivariate statistical model (*P*(data | model)). The statistical model usually takes the form of a regression of species richness on environmental variables, with (Longino & Colwell 2011) or without (Hawkins *et al.* 2003) a predictor variable for geometric constraints. To compare the results from our Bayesian analyses with this traditional, correlative approach to identifying environmental drivers, we carried out multiple regressions of species richness over elevational gradients, as a function of the same environmental variables that we used to interpret the attractors.

Midpoint predictor models. In addition to the Bayesian midpoint attractor model, we built two alternative, stochastic, *midpoint predictor models*—one with and one without geometric constraints—that directly assessed environmental variables as predictors of midpoint density (not species richness) over the elevational gradient. In these models, as in the midpoint attractor model, each empirical range midpoint is placed on the domain (the unit line) stochastically. However, range placement is not driven by a hypothetical attractor, as it is in the Bayesian model. Instead, at each point in the domain, the probability of midpoint placement is directly and linearly proportional to the value of a single, measured, environmental variable, such as temperature or precipitation. Whereas the midpoint attractor model seeks an optimal location and optimal strength for a

hypothetical attractor, the midpoint predictor model assesses the fit of the empirical midpoint data to a probability distribution directly defined by a measured environmental variable. This approach is somewhat akin to the models of Storch *et al.* (Storch *et al.* 2006).and Rahbek *et al.* (Rahbek *et al.* 2007), but contrasts with the traditional MDE model, in which the probability of midpoint occurrence is constant across the domain.

Application of the models. We applied the midpoint attractor model and the two midpoint predictor models to 16 high-quality datasets that recorded the elevational distribution of more than 4500 species of ferns, insects, mammals, or birds in globally distributed localities, mostly in the tropics (Table S1, *Appendix 2*). As we will demonstrate, with or without geometric constraints, the midpoint predictor models generally provide a poor fit to the observed pattern of range midpoints. In contrast, the Bayesian midpoint attractor model simulations consistently produce a good fit to both species richness and midpoint distributions of empirical datasets.

MATERIALS AND METHODS

Empirical Datasets and Data Representation. We applied the midpoint attractor model and the two midpoint predictor models to the 16 datasets detailed in Table S1 (*Appendix 2*). Three groups of datasets included multiple taxa studied on the same gradients: northern Costa Rica, Mt. Wilhelm in Papua New Guinea, and the Border Ranges in Australia. To label the individual datasets, we preface the name of the taxonomic group with the name of the geographic location of the gradient (e.g. “New Guinean ants,” “Costa Rican ferns,” etc.). The biogeographical data from these studies consist of species occurrences recorded at a variable number of sampling elevations (5 to 70 elevations,

median = 8) along each gradient. Each dataset also included measurements for two or more environmental factors along the gradient (Table S1, *Appendix 2*). To facilitate the comparison of results among studies, we rescaled each elevational domain to the [0,1] unit line. Within this domain, we standardized sampling points and converted species occurrence records into an estimated elevational range and midpoint for each species following data preparation protocols detailed in the *Appendix 1, Supplemental Materials and Methods.* Each dataset was represented in two ways: A *midpoint-range plot (Colwell & Hurtt 1994)*, with range size as the ordinate and range midpoint as the abscissa for each range in a dataset (Fig. 2, *right panel*, grey-scale dots and horizontal line segments), and a *species richness plot*, showing the number of overlapping ranges at each of a sequence of sampling locations (elevations) spanning the domain (Fig. 2, *left panel*, black dots).

The Bayesian midpoint attractor model. As outlined in the Introduction, we modeled the midpoint attractor as a Guassian probability density function $N(A, B)$ with two parameters: its mean location A ($0 < A < 1$) on the unit-line domain, and its standard deviation B ($0 < B < 1$) around the attractor (Fig. 1C). Because a Guassian distribution extends from negative to positive infinity, the attractor distribution is truncated at the lower (0) and upper (1) bounds of the domain.

The choice of a unimodal midpoint attractor distribution for an informed Bayesian conjugate prior was based on the empirical prevalence in the published literature of unimodal peaks of species richness (Rahbek 2005), which in turn suggest unimodal midpoint patterns. Our choice of a doubly-truncated Gaussian prior, rather than a prior distribution (e.g. the beta distribution) that declines to zero at the domain limits,, was

based on biological grounds: many species are regularly present at either sea level or mountaintop, their realized distributions directly abutting a domain limit. Such distributions suggest that the fundamental environmental niche is often not fully expressed on a particular elevational gradient.

To model the expected pattern of species richness under the influence of the attractor, each of the empirical ranges in a dataset is placed on the domain stochastically, without replacement, with its midpoint drawn at random from a proposed attractor distribution $N(A, B)$. To enforce the geometric constraint (Fig. 2, *right panel*) and maintain the empirical RSFD, the midpoint is sampled from this distribution only over the interval of feasible midpoints, given the size of each range, such that the range does not extend beyond either the lower or upper domain limit (Colwell and Lees 2000). For a range of length R, this means that the midpoint must lie in the interval $[R/2, 1\text{-}R/2]$. We explored two alternative algorithms for placing ranges within the domain in these stochastic range simulations. The two algorithms differ only in how this placement constraint is achieved.

In Algorithm 1, for a species with an empirical range of length R, a midpoint is simply drawn from $N(A, B)$ on the interval $[R/2, 1\text{-}R/2]$ and assigned to the species. Biologically, this algorithm assumes that the elevational distribution of a typical species fully expresses its environmental niche within the scope of the gradient, because neither its upper nor its lower range limit is likely to reach a domain limit. This algorithm is the equivalent, for the midpoint attractor model, of the *classic MDE model* of Colwell & Hurtt (Colwell & Hurtt 1994) (their Model 2).

In Algorithm 2,, a candidate midpoint is drawn from $N(A, B)$ on the full domain interval [0, 1]. If the candidate midpoint lies within the interval [R/2, 1-R/2], it is assigned to the species and the next species is considered. If it lies to the left of the interval [R/2, 1-R/2], then R/2 is assigned as the midpoint, whereas if the midpoint lies to the right of the interval [R/2, 1-R/2], then 1-R/2 is assigned. The result is that each such shifted range exactly abuts a domain limit. This algorithm is the equivalent, for a one-dimensional domain, of the classic two-dimensional *spreading dye* model of Jetz & Rahbek (Jetz & Rahbek 2001). Biologically, it captures the idea that the environmental niches of species on ecological gradients are often not fully expressed, so that observed distributions are based on truncated niches (Colwell & Rangel 2009; Feeley & Silman 2010). Hence, a better fit to Algorithm 2 than to Algorithm 1 would support the existence of truncated niches.

By design, these stochastic placement algorithms preserve the empirical RSFD, while empirical midpoints are completely ignored. Thus, the correspondence between modeled and empirical patterns of richness, and between empirical and modeled patterns of midpoints, is driven by the location and strength of the attractor.

Just as for empirical richness patterns, the modeled richness at sampling points on the domain is simply the number of stochastically placed ranges that overlap at each sampling point. Because range midpoints are assigned from a statistical distribution (the midpoint attractor), however, each run (realization) of the midpoint attractor simulation yields a somewhat different pattern of richness over the domain. As illustrated in Fig. 2 (*left panel*), over many runs (e.g. 100), a mean result (dark blue line) and a 95% confidence interval (light blue band) can be defined and plotted to compare with

empirical richness (black dots). One simple criterion for evaluating the success of the midpoint attractor model is the proportion of empirical richness values that lie within the 95% confidence interval of modeled richness.

In an approximate Bayesian computational framework (Marjoram *et al.* 2003; Hartig *et al.* 2011)), we used a custom Monte Carlo Markov Chain (MCMC) Gibbs sampler to seek the posterior distribution of model parameters *A* and *B* (and thus the posterior distribution of the location, shape, and truncation points of the Gaussian attractor) that maximized the probability of the model, given the empirical species richness pattern and the empirical RSFD for each dataset. In other words, this procedure finds the location and shape of the midpoint attractor that provides the best fit between modeled richness and empirical richness. The details of the ABC and MCMC procedures appear in the *Appendix 1, Supplemental Materials and Methods*.

In summary, the midpoint attractor model simulates the interaction between a simple, unimodal environmental gradient (the attractor) and the geometric constraints imposed by domain limits. As in the pencil-box analogy (Fig. 1B), because of the constraint, the distribution of predicted midpoints in the model will not always center on the attractor. Thus, we predicted that the closer the modeled attractor lies to one of the two domain limits, the greater would be the expected discrepancy between the location of the attractor and the mean location of range midpoints on the domain. Because of this discordance, if the model fitting procedure is successful, we expected that empirical species richness should correlate more strongly with modeled species richness, as simulated by the midpoint attractor model, than with the attractor itself.

Statistical comparison between modeled and empirical midpoint densities. It is conceivable that the midpoint attractor model could provide a good fit to the empirical species richness pattern, but fail to produce a pattern of range midpoints within the domain that resembles the corresponding empirical pattern of midpoints: the right answer for the wrong reasons. As an independent statistical test of the fit between the modeled and empirical patterns of midpoints and ranges, we divided the constraint triangle of the midpoint-range plot evenly into 16 smaller triangles (Fig. 2, *right panel* and Fig. S4, *Appendix 2*) (Laurie & Silander 2002) and examined the correspondence between modeled and empirical midpoint densities in these triangles with a bootstrap procedure. To assess the prediction that species with small ranges and species with large ranges respond to the same attractor, we repeated the bootstrap procedure separately for larger-ranged species (range size > 0.25 of the domain) and for smaller-ranged species (range size $\leq$ 0.25 of the domain). See *Appendix 1, Supplemental Materials and Methods* for details.

Mapping midpoint attractors onto environmental variables. The Bayesian model optimizes the location and shape of a simple midpoint attractor, without reference to environmental variables measured along each of the gradients. In fact, we know from many sources of evidence that species and species groups respond in complex and often idiosyncratic ways to environmental and elevational gradients (Gotelli *et al.* 2009; Newbery & Lingenfelder 2009; Albert *et al.* 2010; McCain & Grytnes 2010; Presley *et al.* 2011; Sundqvist *et al.* 2011). As is typical for most field studies, only limited environmental data were available for the elevational transects in our datasets, and data for different sets of environmental variables were available for different transects.

In an attempt to characterize attractors statistically in terms of underlying available environmental variables, we carried out (linear) multiple regressions, with AIC-based model selection, for each dataset on each gradient. We treated the attractor as the continuous response variable and the smoothed, interpolated environmental variables as candidate predictor variables. The multiple regression models were fit using the application Spatial Analysis in Macroecology (SAM), version 4.0 (Rangel *et al.* 2010). The data points (elevations) for regression were the same, evenly-spaced points across the unit-line domain that were used to fit each midpoint attractor (see *Appendix 1, Supplemental Materials and Methods*.).

For comparison with approaches traditionally applied to explain species richness patterns, we carried out additional multiple regressions, in a model-selection framework, with (1) empirical richness as the response variable and environmental variables as candidate predictor variables; and (2) empirical richness as the response variable and the modeled attractor as the only predictor variable.

Midpoint predictor models. The midpoint attractor model is, by design, an indirect approach to understanding the drivers of species richness over elevational gradients. As an alternative, direct approach, we designed two explicit *midpoint predictor models*, one with and one without geometric constraints, for the placement of empirical species range midpoints within a domain. Like the midpoint attractor model, these models have two free parameters. For each of these midpoint predictor models and each of the 16 elevational datasets, we assessed the degree to which the empirical distribution of range midpoints within a domain matched that predicted by a stochastic simulation. In contrast with most other studies, including our midpoint attractor model, the midpoint predictor

models consider only the frequency distribution of species midpoints along the elevational gradient, and not the resulting species richness arising from the overlap of species ranges. Details of the two midpoint predictor models and our approach to model evaluation appear in *Appendix 1, Supplemental Materials and Methods*.

RESULTS

Midpoint attractors and geometric constraints. Fig. 2 shows the empirical data and the fitted midpoint attractor model for the Costa Rican arctiine moth dataset. The corresponding graphical results for the other 15 datasets appear in Figs. 3 and 4, organized by locality and arranged to facilitate comparisons between taxonomically and geographically related datasets. We emphasize that each of these results represents a single, illustrative example from the Bayesian posterior distribution of the midpoint attractor, as specified by optimized parameters *A* and *B*, for the corresponding dataset. For each dataset, nearby values of these parameters produce similar graphs. The spreading dye algorithm (Algorithm 2) consistently yielded a fit between modeled and empirical richness that was at least as good, and often better, than the classic approach (Algorithm 1). Consequently, we used the spreading dye algorithm for all datasets in the final models (Table S2).

Table S2 (*Appendix 2*) displays the quantitative results for midpoint attractor parameters, and for each, the results for the independent statistical comparisons between modeled and empirical midpoint density patterns within the geometric constraint triangle (*right panel* for each dataset in Figs. 2, 3, and 4). For 14 of the 16 datasets, the test affirms a highly significant (mean $P < 0.002$) correspondence between empirical and

modeled midpoint density patterns. The two exceptions (Costa Rican ferns and North American butterflies), instructive in their own right, are discussed in *Appendix 1*, *Supplemental Discussion*. The comparison of modeled and empirical midpoint densities for large-ranged *vs*. small-ranged species confirmed the expectation that both large and small ranges are equally well fit by the same midpoint attractor model for most datasets (11 of 16).

The quantitative results in Table S2 (*Appendix 1*) offer strong evidence of a key role for geometric constraints in the modeled patterns of richness. As predicted (*Materials and Methods*), the closer the modeled attractor is to a domain limit, the greater the discrepancy between the location of the attractor and the mean location of range midpoints on the domain (Fig. 5). In terms of the pencil-box analogy (Fig. 1B), the closer the magnet is set to one end of the box, the further the average pencil midpoint is forced away from the box end.

The fitted standard deviation of the midpoint attractor (parameter *B* in the simulations), an inverse measure of the strength of the attractor, varied from 0.023 for Costa Rican ants to 0.476 for North American butterflies (Table S2, *Appendix 2*), The location of the midpoint attractor (parameter *A*) on the unit-line domain ranged from 0.065 for Costa Rican ants, with nearly monotonically declining richness with elevation, to several datasets with *A* near 0.5 (Costa Rican ferns and geometrid moths, North American butterflies, and Australian moths and their parasitoids) to 0.742 (Australian leaf-miners, on a short, 1100 m gradient). When translated to absolute elevation, *A* and *B* vary even more strikingly, because the datasets vary from 1100 m to 4095 m in elevational scope (Table S1, *Appendix 1*). When the best-fit attractor lies near the center

of the domain, as it does for the Costa Rican ferns (Fig. 2) or North American butterflies (Fig. 4), the modeled pattern of richness may be quite symmetrical—but so is the expected pattern from a simpler MDE model of geometric constraints with no environmental drivers. We discuss this issue in detail in *Appendix 1, Supplemental Discussion*.

How well did the model perform in simulating empirical richness? The first two graphs for each dataset in Fig. S1 (*Appendix 2*) show: (1) the regression of empirical richness on the modeled midpoint attractor, and (2) the regression of empirical richness on modeled richness. Table S3 (*Appendix 2*) provides the corresponding statistical results. From these results, we can assess the expectation (*Materials and Methods*) that empirical species richness should correlate more strongly with modeled species richness, as simulated by the midpoint attractor model, than with the attractor itself. This expectation was borne out in 12 of the 16 datasets. The four exceptions, which demonstrate that this pattern is not an inevitable result of the fitting method, are detailed in *Appendix 1, Supplemental Results*.

Mapping midpoint attractors onto environmental variables. Using the results from the midpoint attractor model, the third and fourth graph for each dataset in Fig. S1 (*Appendix 2*), illustrate results for all 16 datasets from the AIC-guided analyses of (1) the regression of modeled midpoint attractors on environmental variables, and (2) the regression of empirical richness on environmental variables. Table S3 (*Appendix 2*) provides the corresponding statistical results and comparisons.

The environmental variables that best explained the modeled midpoint attractor often differed from the environmental variables that best predicted observed species

richness. Only two of the 16 datasets yielded an identical environmental predictor model (or model group, when ΔAIC was < 3 between alternatives), in terms of predictor variables included, for attractor and for species richness. However, the model with the lowest absolute AIC matched in 9 of the 16 datasets if AIC-grouped models were ignored (illustrated in Fig. S1, *Appendix 2*,).

Midpoint predictor models. For each dataset, the same environmental variables assessed in interpreting midpoint attractors *(Table S3 and Fig. S1, Appendix 2*) were tested for the two midpoint predictor models (direct environmental predictors, with and without geometric constraints). Across all data sets, 98 of 112 statistical tests strongly rejected the null hypothesis that modeled midpoints resemble the empirical ones, with *P* < 0.001 in nearly every case (Table S4, *Appendix 2*). Only four of the 16 data sets showed an acceptable fit (P > 0.05) to either of the midpoint predictor models. But these datasets were, not coincidentally, the four smallest, in terms of number of species (Australian leaf-miners and parasitoids, Costa Rican and North American mammals), and thus had the weakest statistical power to reject the null hypothesis.

DISCUSSION

Although the elevational richness patterns successfully modeled in this study varied widely in shape and location on the domain, the midpoint attractor model successfully reproduced not only taxon-specific peaks of species richness, but also their underlying empirical midpoint distributions (Figs. 2, 3, and 4). The strong signature of geometric constraints in these results (Fig. 5) shows that the midpoint attractor, alone, is not responsible for the excellent fit of model to data. Instead, the seamless integration of

attractor and constraints allows the model to generate patterns ranging from nearly monotonic declines of species richness to perfectly symmetric mid-elevation humps.

Because the specific environmental and historical factors underlying the notion of "favorability" are not explicitly incorporated in our model, it might be tempting to dismiss these results as purely descriptive curve-fitting. On the contrary, by revealing an underlying gradient of favorability, we argue that our Bayesian midpoint attractor model offers a unifying approach to elevational richness gradients that has not been achieved by traditional, *ad hoc* statistical analyses of richness gradients, based on correlations with environmental drivers (Gotelli et al. 2009).

Constructing the midpoint attractor model in a Bayesian framework was not a matter of convenience, interpretation, or fashion, but rather a logical necessity. Given the conjecture that a taxon-specific, location-specific, underlying gradient of favorability, interacting with geometric constraints, could explain elevational richness patterns, the appropriate way forward was to maximize the probability of a general, underlying model, challenged with a plethora of contrasting datasets, a fundamentally Bayesian approach.

Datasets with many ranges abutting the low-elevation domain limit (e.g. Costa Rican ants, Fig. 2, and Bornean geometrid and sphingid moths, Fig. 4) or the high-elevation domain limit (Australian leaf-miner parasitoids and North American butterflies, Fig. 4) strongly suggest an unexpressed potential for some species to prosper in environmental conditions more extreme than those at the lower or upper domain limit. In other words, range limits in geographical space, forced by the domain boundaries (e.g. sea level or mountaintop), may not coincide with niche limits in niche space for such species (Colwell & Rangel 2010). The excellent performance of the doubly-truncated

Gaussian attractor, chosen as an informed prior, and our finding that Algorithm 2 (spreading dye) provided a better fit than Algorithm 1 (classic) together offer strong support for the inference that ranges that abut domain boundaries represent truncated niches at the extremes of elevational gradients.

With or without geometric constraints, the midpoint predictor models, which assessed empirical environmental factors as candidate midpoint predictors, fit observed elevational midpoint distributions very poorly (Table S4, *Appendix 2*), despite incorporating the empirical RSFD and having the same number of free parameters as the midpoint attractor model. Although the familiar correlations, in the literature, between species richness and temperature, precipitation, and other environmental variables are often interpreted as evidence for causal relationships, these statistical correlations do not represent actual models of cause-and-effect. For the datasets in this study, the seemingly intuitive hypothesis that environmental conditions should predict the location of species' range midpoints failed to account for most observed patterns. How can we reconcile this failure of the midpoint predictor model with the success of the midpoint attractor model? At least three, non-exclusive explanations are possible: (1) We might have used the "wrong" environmental variables; (2) we might have analyzed the right variables, but we had the wrong functional form; or (3) lineage diversification with strong niche conservatism may have produced spatial concentrations of range midpoints in narrowly-defined environments (see *Appendix 1, Supplemental Discussion).*

The environmental and historical factors that underlie midpoint attractors in nature are likely to be complex, presenting a challenge for future research. But we conjecture that our approach, in which a modeled midpoint attractor drives the location of

species ranges placed stochastically within a bounded domain, may prove more fruitful than further attempts to directly link patterns of species richness along bounded gradients with environmental factors.

Acknowledgments

This study had its origins at a workshop in Ceske Budejovice, Czech Republic, in August, 2013, organized by V. Novotny and funded by the Czech Ministry of Education and the European Social Fund (CZ.1.07/2.3.00/20.0064). Author support: CAPES Ciência sem Fronteiras (Brazil) (R.K.C.); U. S. NSF DEB 1257625, DEB 1144055, & DEB 1136644 (N.J.G.); NSF DEB 1354739 (Project ADMAC) (J.T.L.); NSF DEB 841885 (J.M. & V.N); Griffith University & Australian Postgraduate Research Awards (L.A.A. and S.C.M.); Australian Research Council DP140101541 & Yayasan Sime Darby (T.M.F.); German DFG Br 2280/1-1, Fi547/5-1, & FOR 402/1-1 (G.B & K.F.); DFG & German Academic Exchange Service DAAD (J.K.); DFG, Swiss National Fund, & Claraz Schenkung (M.K. & S.N); Czech Science Foundation 14-36098G & 14-32024 (T.M.F., P.K., & K.S.), 13-10486S (J.M. & V.N); National Natural Science Foundation of China 31370620 (X.W.); UK Darwin Initiative 19-008 (J.M. and V.N.); & IBISCA (T.M.F., K.S, & L.S). We are grateful to Paul Lewis for consultation on Bayesian methods.

References

Ahrens, C.D. (2006). *Meteorology today (8th ed.)*. Brooks/Cole Publishing.

Albert, C.H., Thuiller, W., Yoccoz, N.G., Soudant, A., Boucher, F., Saccone, P. *et al.* (2010). Intraspecific functional variability: extent, structure and sources of variation. *J. Ecol.*, 98, 604-613.

Allen, A.P., Gillooly, J.F. & Brown, J.H. (2007). Recasting the species-energy hypothesis: the different roles of kinetic and potential energy in regulating biodiversity. *Scaling biodiversity*, 1.

Ashton, L.A., Odell, E.H., Burwell, C.J., Maunsell, S.C., Nakamura, A., McDonald, W.J.F. *et al.* (In press.). Elevational patterns of moth diversity in tropical and subtropical Australia. *Austral Ecol.*

Beck, J., Holloway, J.D., Khen, C.V. & Kitching, I.J. (2012). Diversity partitioning confirms the importance of beta components in tropical rainforest Lepidoptera. *Am. Nat.*, 180, E64-E74.

Beck, J. & Kitching, I.J. (2009). Drivers of moth species richness on tropical altitudinal gradients: a cross-regional comparison. *Global Ecol. Biogeogr.*, 18, 361-371.

Bellwood, D., Hughes, T., Connolly, S. & Tanner, J. (2005). Environmental and geometric constraints on Indo-Pacific coral reef biodiversity. *Ecol. Lett.*, 8, 643-651.

Brehm, G., Colwell, R.K. & Kluge, J. (2007). The role of environment and mid-domain effect on moth species richness along a tropical elevational gradient. *Global Ecology & Biogeography*, 16, 205-219.

Cardelús, C.L., Colwell, R.K. & Watkins, J.E. (2006). Vascular epiphyte distribution patterns: explaining the mid-elevation richness peak. *J. Ecology*, 94, 144-156.

Colwell, R.K. (2008). RangeModel: Tools for exploring and assessing geometric constraints on species richness (the mid-domain effect) along transects. *Ecography*, 31, 4-7.

Colwell, R.K. & Hurtt, G.C. (1994). Nonbiological gradients in species richness and a spurious Rapoport effect. *Am. Nat.*, 144, 570-595.

Colwell, R.K. & Lees, D.C. (2000). The mid-domain effect: geometric constraints on the geography of species richness. *Trends in Ecology and Evolution*, 15, 70-76.

Colwell, R.K., Rahbek, C. & Gotelli, N. (2004). The mid-domain effect and species richness patterns: what have we learned so far? *Am. Nat.*, 163, E1-E23.

Colwell, R.K., Rahbek, C. & Gotelli, N. (2005). The mid-domain effect: there's a baby in the bathwater. *Am. Nat.*, 166, E149–E154.

Colwell, R.K. & Rangel, T.F. (2009). Hutchinson's duality: the once and future niche. *PNAS* 106, 19651-19658.

Colwell, R.K. & Rangel, T.F. (2010). A stochastic, evolutionary model for range shifts and richness on tropical elevational gradients under Quaternary glacial cycles. *Phil. Trans. R. Soc. London Ser. B*, 365 3695–3707.

Currie, D., Mittelbach, G., Cornell, H., Field, R., Guegan, J., Hawkins, B. *et al.* (2004). Predictions and tests of climate-based hypotheses of broad-scale variation in taxonomic richness. *Ecol. Lett.*, 7, 1121-1134.

Currie, D.J. & Kerr, J.T. (2008). Tests of the mid-domain hypothesis: a review of the evidence. *Ecol. Monogr.*, 78, 3-18.

Davies, R.G., Orme, C.D.L., Storch, D., Olson, V.A., Thomas, G.H., Ross, S.G. *et al.* (2007). Topography, energy and the global distribution of bird species richness. *Proc. R. Soc. B-Biol. Sci.*, 274, 1189-1197.

Dunn, R.R., Colwell, R.K. & Nilsson, C. (2006). The river domain: why are there more species halfway up the river? *Ecography*, 29, 251-259.

Dunn, R.R., McCain, C.M. & Sanders, N. (2007). When does diversity fit null model predictions? Scale and range size mediate the mid-domain effect. *Global Ecology & Biogeography*, 3, 305-312.

Fan, Y. & van den Dool, H. (2008). A global monthly land surface air temperature analysis for1948–present. *J. Geophys. Res*, 113, D01103.

Feeley, K.J. & Silman, M.R. (2010). Biotic attrition from tropical forests correcting for truncated temperature niches. *Global Change Biol.*, 16, 1830-1836.

Forister, M.L., McCall, A.C., Sanders, N.J., Fordyce, J.A., Thorne, J.H., O'Brien, J. *et al.* (2010). Compounded effects of climate change and habitat alteration shift patterns of butterfly diversity. *Proc. Natl. Acad. Sci. U. S. A.*, 107, 2088-2092.

Gelman, A., Carlin, J.B., Stern, H.S., Dunson, D.B., Vehtari, A. & Rubin, D.B. (2013). *Bayesian data analysis*. CRC press.

Gotelli, N., Anderson, M.J., Arita, H.T., Chao, A., Colwell, R.K., Connolly, S.R. *et al.* (2009). Patterns and causes of species richness: a general simulation model for macroecology. *Ecol. Lett.*, 12, 873-886.

Graham, C.H., Carnaval, A.C., Cadena, C.D., Zamudio, K.R., Roberts, T.E., Parra, J.L. *et al.* (2014). The origin and maintenance of montane diversity: integrating evolutionary and ecological processes. *Ecography*, 37, 711-719.

Grinnell, J. & Storer, T.I. (1924). *Animal life in the Yosemite: an account of the mammals, birds, reptiles, and amphibians in a cross-section of the Sierra Nevada*. University of California Press.

Grytnes, J. (2003). Ecological interpretations of the mid-domain effect. *Ecol. Lett.*, 6, 883-888.

Grytnes, J.A., Beaman, J.H., Romdal, T.S. & Rahbek, C. (2008). The mid-domain effect matters: simulation analyses of range-size distribution data from Mount Kinabalu, Borneo. *J. Biogeogr.*, 35, 2138-2147.

Hartig, F., Calabrese, J.M., Reineking, B., Wiegand, T. & Huth, A. (2011). Statistical inference for stochastic simulation models–theory and application. *Ecol. Lett.*, 14, 816-827.

Hawkins, B.A., Field, R., Cornell, H.V., Currie, D.J., Guégan, J.-F., Kaufmann, D.M. *et al.* (2003). Energy, water, and broad-scale geographic patterns of species richness. *Ecology*, 84, 3105–3117.

Hubbell, S.P. (2001). *The unified theory of biodiversity and biogeography*. Princeton University Press, Princeton, N. J.

Jetz, W. & Rahbek, C. (2001). Geometric constraints explain much of the species richness pattern in African birds. *PNAS*, 98, 5661-5666.

Kluge, J., Kessler, M. & Dunn, R.R. (2006). What drives elevational patterns of diversity? A test of geometric constraints, climate and species pool effects for pteridophytes on an elevational gradient in Costa Rica. *Global Ecology & Biogeography*, 15, 358-371.

590Laurie, H. & Silander Jr., J.A. (2002). Geometric constraints and spatial pattern of species
591 richness: critique of range-based null models. *Divers. Distrib.*, 8, 351-364.
592Lees, D.C., Kremen, C. & Andriamampianina, L. (1999). A null model for species
593 richness gradients: bounded range overlap of butterflies and other rainforest
594 endemics in Madagascar. *Biol. J. Linn. Soc.*, 67, 529-584.
595Letten, A.D., Kathleen Lyons, S. & Moles, A.T. (2013). The mid-domain effect: it's not
596 just about space. *J. Biogeogr.*, 40, 2017-2019.
597Lomolino, M.V. (2001). Elevational gradients of species density: historical and
598 prospective views. *Global Ecol. Biogeogr.*, 10.
599Longino, J.T., Branstetter, M.G. & Colwell, R.K. (2014). How Ants Drop Out: Ant
600 Abundance on Tropical Mountains. *PLoS One*, 9, e104030.
601Longino, J.T. & Colwell, R.K. (2011). Density compensation, species composition, and
602 richness of ants on a neotropical elevational gradient. *Ecosphere*, 2(3):art29,
603 doi:10.1890/ES10-00200.1.
604Marjoram, P., Molitor, J., Plagnol, V. & Tavaré, S. (2003). Markov chain Monte Carlo
605 without likelihoods. *Proc. Natl. Acad. Sci. U. S. A.*, 100, 15324.
606Maunsell, S.C., Burwell, C.J., Morris, R.J., McDonald, W.J., Edwards, T., Oberprieler, R.
607 *et al.* (In press.). Leaf miner host plant use and elevation in Australian subtropical
608 rainforest. *Austral Ecology.*
609Maunsell, S.C., Kitching, R.L., Burwell, C.J. & Morris, R.J. (2015). Changes in host–
610 parasitoid food web structure with elevation. *J. Anim. Ecol.*, 84, 353-363.
611McCain, C. (2005). Elevational gradients in diversity of small mammals. *Ecology*, 86,
612 366-372.

McCain, C.M. (2004). The mid-domain effect applied to elevational gradients: species richness of small mammals in Costa Rica. *J. Biogeogr.*, 31, 19-31.

McCain, C.M. (2007). Could temperature and water availability drive elevational species richness patterns? A global case study for bats. *Global Ecology & Biogeography*, 16, 1-13.

McCain, C.M. (2009). Vertebrate range sizes indicate that mountains may be 'higher' in the tropics. *Ecol. Lett.*, 12, 550-560.

McCain, C.M. & Grytnes, J.A. (2010). Elevational gradients in species richness. *eLS*.

Moses, J. (2015). Tropical elevational gradient in ants (Hymenoptera: Formicidae): Diversity patterns, food preferences and nutrient redistribution rates on Mt Wilhelm, Papua New Guinea. MSc Thesis, University of Papua New Guinea, Port Moresby., p. 85 pp.

Newbery, D. & Lingenfelder, M. (2009). Plurality of tree species responses to drought perturbation in Bornean tropical rain forest. In: *Forest Ecology*. Springer, pp. 147-167.

Presley, S.J., Willig, M.R., Bloch, C.P., Castro-Arellano, I., Higgins, C.L. & Klingbeil, B.T. (2011). A complex metacommunity structure for gastropods along an elevational gradient. *Biotropica*, 43, 480-488.

Prevedello, J.A., Figueiredo, M.S., Grelle, C.E. & Vieira, M.V. (2013). Rethinking edge effects: the unaccounted role of geometric constraints. *Ecography*, 36, 287-299.

Rahbek, C. (1995). The elevational gradient of species richness: a uniform pattern? *Ecography*, 19, 200-205.

Rahbek, C. (2005). The role of spatial scale in the perception of large-scale species-richness patterns. *Ecol. Lett.*, 8, 224-239.

Rahbek, C., Gotelli, N., Colwell, R.K., Entsminger, G.L., Rangel, T.F.L.V.B. & Graves, G.R. (2007). Predicting continental-scale patterns of bird species richness with spatially explicit models. *Proceedings of the Royal Society of London Series B*, 274, 165-174.

Rangel, T.F., Diniz Filho, J.A.F. & Bini, L.M. (2010). SAM: a comprehensive application for Spatial Analysis in Macroecology. *Ecography*, 33, 46–50.

Rangel, T.F.L.V.B. & Diniz-Filho, J.A.F. (2005). An evolutionary tolerance model explaining spatial patterns in species richness under environmental gradients and geometric constraints. *Ecography*, 28, 253-263.

Sam, K. & Koane, B. (2014). New avian records along the elevational gradient of Mt. Wilhelm, Papua New Guinea. Bulletin of the British Ornithologists' Club 134, 116-133.

Sam, L. (2011). Responses of butterfly (Lepidoptera) communities along an altitudinal forest gradient in Papua New Guinea. MSc Thesis, University of Papua New Guinea, Port Moresby, p. 66 pp.

Storch, D., Davies, R.G., Zajicek, S., Orme, C.D.L., Olson, V., Thomas, G.H. *et al.* (2006). Energy, range dynamics and global species richness patterns: reconciling mid-domain effects and environmental determinants of avian diversity. *Ecol. Lett.*, 9, 1308-1320.

Sundqvist, M.K., Giesler, R., Graae, B.J., Wallander, H., Fogelberg, E. & Wardle, D.A. (2011). Interactive effects of vegetation type and elevation on aboveground and belowground properties in a subarctic tundra. *Oikos*, 120, 128-142.

Team, R.C. (2014). *R: A language and environment for statistical computing.* . R Foundation for Statistical Computing, Vienna, Austria. , URL http://www.R-project.org/.

Tiwari, M., Bjorndal, K.A., Bolten, A.B. & Bolker, B.M. (2005). Intraspecific application of the mid-domain effect model: spatial and temporal nest distributions of green turtles, *Chelonia mydas*, at Tortuguero, Costa Rica. *Ecol. Lett.*, 8, 918-924.

Tvardikova, K. (2013). Trophic relationships between insectivorous birds and insect in Papua New Guinea. . Thesis Series, No. 9. University of South Bohemia, Faculty of Science, School of Doctoral Studies in Biological Sciences, České Budějovice, Czech Republic, p. 184 pp.

Wang, X. & Fang, J. (2012). Constraining null models with environmental gradients: a new method for evaluating the effects of environmental factors and geometric constraints on geographic diversity patterns. *Ecography*, 35, 1147–1159.

Wright, S.J., Muller-Landau, H. & Schipper, J. (2009). The future of tropical species on a warmer planet. *Conserv. Biol.*, 23, 1418-1426.

Wu, Y., Colwell, R.K., Han, N., Zhang, R., Wang, W., Quan, Q. *et al.* (2014). Understanding historical and current patterns of species richness of babblers along a 5000-m subtropical elevational gradient. *Global Ecol. Biogeogr.*, 1167-1176.

Wu, Y., Yang, Q., Wen, Z., Xia, L., Zhang, Q. & Zhou, H. (2012). What drives the species richness patterns of non-volant small mammals along a subtropical elevational gradient? *Ecography*, 36, 185-196.

Figure Captions (Main Text)

*(**Note:** In the all-in-one pdf prepared for peer review, each caption appears in context with the corresponding figure at the end of the file.)*

APPENDICES

Midpoint attractors and species richness: Modeling the interaction between environmental drivers and geometric constraints

APPENDIX 1: SUPPLEMENTAL TEXT

APPENDIX 2: SUPPLEMENTAL TABLES AND FIGURES

*(**Note:** In the all-in-one pdf prepared for peer review, each caption appears in context with the corresponding figure at the end of the file.)*

*(**Note**: References are integrated with Main Text references)*

APPENDIX 1: SUPPLEMENTAL TEXT

SUPPLEMENTAL INTRODUCTION

Integrating geometric constraints with environmental and historical explanations for patterns of species richness

Beginning with Lees *et al.* (1999) and Jetz and Rahbek (2001), many authors have taken a statistical approach, treating “pure” MDE model predictions as candidate predictor variables. In most of these studies, the observed range-size frequency distribution (RSDF) was sampled without replacement to generate the MDE model predictions of expected species richness at each location in the domain (Colwell *et al.* 2004, 2005). The

710MDE predictions and standard environmental variables were then used together in
711traditional correlative modeling of species richness patterns. Increasingly rigorous
712versions of this statistical approach have incorporated formal model selection, spatial
713statistics, and assessment of multicollinearity (Bellwood *et al.* 2005; Davies *et al.* 2007;
714Wu *et al.* 2012).

715 Several studies have integrated constraints and drivers directly, incorporating the
716interacting effects of geometric constraints and environmental drivers on species richness
717(Gotelli *et al.* 2009) by using environmental variables to condition probabilities of range
718placement and expansion within a spatially bounded domain (Storch *et al.* 2006; Rahbek
719*et al.* 2007), thus relaxing the assumption of a pure MDE model that parts of the domain
720are environmentally identical. These models were also conditioned on the empirical range
721size frequency distribution (RSFD). In contrast, Grytnes et al. (Grytnes *et al.* 2008)
722modeled plant richness on a bounded elevational gradient by drawing range sizes from
723theoretical distributions and range midpoints from a probability distribution fitted directly
724to the observed richness gradient.

725 Rangel and Diniz-Filho (2005) built a stochastic, mechanistic model that
726integrates speciation, range expansion, and extinction on a bounded, monotonic
727environmental “favorability” gradient, without reference to empirical data. The model is
728effectively a spatially explicit version of the neutral model (Hubbell 2001) in a one-
729dimensional bounded domain, but with an underlying environmental gradient. The
730Rangel and Diniz-Filho (2005) model generated off-center species richness peaks that
731emerged from the interaction between the gradient and the geometric constraints (Colwell
732& Rangel 2009). Without the environmental gradient— or with a very weak gradient—

Rangel and Diniz-Filho's model generated a peak of species richness in the center of the domain that was qualitatively similar to the predictions of the simple MDE model.

Wang and Fang (Wang & Fang 2012) developed a third approach. They fitted a multiple regression model of species richness as a response to environmental variables, but they used only the subset of species with the smallest geographic ranges to parameterize the model. They reasoned that the placement of small-ranged species within a bounded domain is little affected by the location of range boundaries, so that, for this subset of taxa, correlations of species richness and environmental variables will not be distorted by geometric constraints. They then used the resulting model coefficients, together with the empirical RSFD, to simulate the placement of range midpoints of the larger-ranged species within the bounded domain. They showed that a single environmental model, combined with strong geometric constraints, best explains the species richness of both small- and large-ranged plant species along elevational gradients in China.

SUPPLEMENTAL MATERIALS AND METHODS

Dataset selection and preparation

As a criterion for inclusion in this study, we applied the rule (McCain 2007; McCain 2009) that at least 70% of the physical gradient between sea level and mountaintop must have been sampled and at least four environmental variables had been reported for the gradient.

Each of the 16 datasets (Table S1) was prepared in the same way. Domain limits were defined as sea level and the highest elevation on the mountain massif upon which

755the gradient was located. This domain was converted to the unit line, and all empirical
756sampling elevations were proportionally scaled within this [0,1] domain. Environmental
757variables (Table S1) were resampled, as necessary, after smoothing with cubic spline
758interpolation, using the *splinefun* function in R, version 3.1.1 (Team 2014).

759 If the highest elevation at which a species was recorded was not at the highest
760sampling location, the upper boundary for that species' range was estimated to occur
761halfway between the highest elevation of recorded occurrence and the next higher
762sampling elevation. If the highest elevation at which a species was recorded at was the
763highest sampling elevation, the upper boundary of that species' range was estimated to
764occur half-way between that sampling elevation and the upper limit of the domain. The
765lower boundary for each range was treated analogously, being extended halfway to the
766next lower sampling elevation or halfway to the lower domain limit (sea level), if a
767species was recorded at the lowest sampling elevation, but that elevation was not the
768domain limit. The ranges of each species found at only one sampling elevation were
769treated similarly. Otherwise, these point ranges would have had a zero range, and would
770have been lost from the model. We assumed that the occurrence of each species was
771continuous between its estimated upper and lower recorded range boundaries. These
772range-adjustment procedures and assumptions have been widely used in previous studies
773(Cardelús *et al.* 2006; Longino *et al.* 2014)

774 The protocol for range adjustment, described above, leaves most datasets without
775any empirical ranges that actually reach the domain boundaries, resulting in zero
776estimated empirical richness at one or both limits of the domain. A few zeroes are real
777(e.g., ants do not occur at very high elevations in the Costa Rica and New Guinea

gradients), but most others are artifacts of the location of original sampling elevations and the range estimation protocol. Data providers (Table S1) were asked in each case whether such zeroes in their data sets were real or artifactual. If real, zero richness at the domain endpoint (and in some cases adjacent sampling points) was plotted and included in analyses; if artifactual, we proportionally adjusted all empirical range midpoints so that ranges nearest to the domain limit exactly reached it. The shifts needed to achieve this adjustment, which effectively shifts the domain boundary slightly, were consistently very small (0.002 to 0.02 on the unit line).

To cope with the wide variation among datasets in number and spacing (often not uniform) of empirical sampling points, we took a mixed approach. For fitting the attractor (see below), we used a series of 11 evenly spaced sampling locations across the entire unit line (domain), including both ends of the domain (0 and 1), for all datasets except the New Guinea group. The New Guinea transect was sampled in the field at 8 evenly-spaced elevations, so with the domain ends added, we used 10 sampling points for fitting the attractor in those datasets. For plotting model results (main text Figs. 2, 3, and 4), we used the original sampling points for datasets with fewer than 11 original points (eight points for the four Papua New Guinea datasets, five for the three Australia datasets, and six for North American butterflies), and 11 points for all other datasets.

The Bayesian Midpoint Attractor model

The MCMC sampler and richness pattern simulation. We designed a simple MCMC Gibbs sampler (Gelman *et al.* 2013) to select (*A*, *B*) pairs for the mean (*A*) and standard deviation (*B*), the parameters of the Gausian midpoint attractor, with the objective of simulating the richness pattern over the domain for a particular empirical dataset, using

only the range-size frequency distribution (RSFD) as input. Empirical midpoints were completely ignored for the simulations. The goodness of fit between modeled and empirical richness was then assessed for each simulation, as detailed below.

Running the simulation. For each candidate (*A*, *B*) pair, each empirical range was placed stochastically on the domain, without replacement, using either Algorithm 1 or 2 (*Main text, Materials and Methods*). The modeled richness was recorded for *L* (10 or 11, see above) evenly spaced sampling locations across the domain, always including both ends of the domain (0 and 1). The process was repeated *M* (= 100) times, for the same (*A*, *B*) pair. The mean richness for each of the *L* sampling points on the domain was then computed, among the *M* runs, to estimate the expected richness pattern, given the (*A*, *B*) pair and the empirical RSFD.

Measuring goodness-of-fit. The next step in the MCMC assessed the goodness-of-fit (GOF) between the empirical richness pattern and the mean modeled pattern, for a given candidate (*A*, *B*) pair, at the *L* sampling points. We applied three alternative GOF measures: (1) *r*, the Pearson product-moment correlation coefficient (but only when positive), squared; (2) the chi-squared statistic computed on standardized richness (the richness at each sampling point, divided by total richness at all *L* points), treating the empirical richness as “expected” and the modeled richness as “observed” (as is customary in Bayesian modeling); and (3) the two-sample Kolmogorov-Smirnov (K-S) statistic. Note that none of these measures can be used in this way to yield a probability test of significance; they are simply mathematically suitable measures of GOF for richness patterns. The protocol for choosing the best GOF for each dataset is described, in context, in the next section.

Sampling the parameter space. Using the procedure just described, the MCMC sampler tested a series of (*A*, *B*) pairs. At each step in this process, a candidate (*A*, *B*) pair was proposed by drawing a new value for *A* and a new value for *B* from uniform distributions [$0 < A < 1$] and [$0 < B < 1$]. In Bayesian terms, *A* was an uninformative hyperprior, with the full [0,1] domain sampled uniformly for the location of the mean (*A*). For the standard deviation (*B*), we also set the upper limit at 1 because this value produces a spatial pattern of richness broader and flatter than any empirical richness pattern we have seen; thus the distribution of hyperprior *B* incorporated this prior information. (An even higher limit for *B* could have been used, but the results would not have changed.)

The candidate (*A*, *B*) pair was evaluated by running the simulation (*M* times) and assessing goodness-of-fit (GOF) between the mean modeled richness (averaged among *M* runs) and empirical richness (as described above). If the GOF for the candidate (*A*, *B*) pair was better, or not much worse, than the GOF for the previous pair, the new pair was added to the chain and the process repeated. The criterion for "not much worse" is important. If only parameter sets (*A*, *B* pairs) that yield a better fit than the previous step were to have been kept, the chain might have become stuck on a local GOF "peak" in the parameter space, and failed to detect a higher peak nearby.

The criterion for accepting a candidate (*A*, *B*) pair in our model was the *threshold-for-acceptance ratio T*, between the GOF of the candidate (*A*, *B*) pair and the GOF of the previous (*A*, *B*) pair in the chain. The ratio *T* was compared to a uniform random number on the interval [0,1] (Gelman *et al.* 2013). If *T* was greater than this number, the candidate (*A*, *B*) pair was accepted and the chain continued; if *T* was smaller than this number, the candidate pair was rejected, and a new candidate pair was proposed. In this

way, better pairs ($T > 1$) were always accepted, and some not-as-good pairs ($T < 1$) were also accepted, ensuring a better sampling of the parameter space.

For each dataset, $C = 200$ to 500 candidate pairs were tried, and the accepted (A, B) pairs (the chain) were tabulated, each with its GOF and step number in the chain. When the process was complete, the accepted (A, B) pairs were plotted (Fig. S3), and ranked by their GOF (largest to smallest for Pearson and Kolmogorov-Smirnov GOFs, smallest to largest for the chi-squared GOF).

For each dataset, when results differed substantially between the two stochastic range placement algorithms in the Bayesian attractor model (*Main text, Materials and Methods*), GOF measures were used to choose the better of the two algorithms. When results differed substantially among GOF measures for the same algorithm for a particular dataset, the best result was chosen based on overall deviation of empirical points from the 95% confidence intervals of the model. Based on this procedure, Pearson correlation emerged as the most successful GOF (13 of 16 datasets), with chi-squared providing a better result in two cases (Australian leaf-miners and Bornean geometrid moths), and Kolmogorov-Smirnov in one case (North American mammals).

Using the approximate best fit (A, B) pair from the Bayesian posterior distribution arising from MCMC sampling, the model was run once to generate species richness and midpoint density values for analysis and illustration, with 100 replications. For a given (A, B) pair, the resulting pattern was highly repeatable, and nearby (A, B) pairs from the posterior distribution gave similar results. We also visualized the fit by plotting modeled richness as a function of empirical richness, for the evenly-spaced sampling points used in the Bayesian parameter search (or for the empirical sampling sites for the New

Guinean, Australian, and North American butterfly datasets), and measured the fit by computing ordinary least squares (OLS) R^2 for this relationship (Fig. S1 and Table S2, *Appendix 2*). Because the number of sampling points is somewhat arbitrary and successive points are not independent, no *P*-value can be assigned to this measure of fit.

Statistical comparison between modeled and empirical midpoint densities

As explained in the main text (*Materials and Methods*), the empirical midpoints and ranges were plotted in a midpoint-range plot, with the classic constraint triangle subdivided into 16 similar isosceles sub-triangles (Fig. S4, *Appendix 2*; main text Figs. 2, 3, and 4, *right panel for each dataset*). As a statistic of correspondence between empirical and modeled midpoint density distributions in the 16 sub-triangles, we used the rank of the observed OLS R^2, computed for the 16 sub-triangles, among 999 values from a bootstrap resampling procedure. Raw R^2 is inflated by the fact that the total number of points within each of the four rows of smaller triangles (triangle 1, triangles 2-4, 5-9, and 10-16 in Fig. S4) is identical for modeled and empirical distributions. These numbers are identical because the empirical RSFD is used, for each dataset, to construct the modeled distribution.

To establish an unbiased sampling distribution, the midpoints within each of the lower three rows of triangles were shuffled at random among the triangles in each row (e.g. among triangles 5-9) and R^2 computed between the empirical counts and the shuffled counts for all 16 triangles, 999 times. (Triangle 1 is constrained to have exactly the same number of points for modeled and empirical data, so no shuffling can be done.) The ordinal *P*-value for the modeled *vs.* empirical R^2 was then based on its rank among the 999 bootstrapped values of R^2.

We repeated the bootstrap procedure outlined above, separately for larger-ranged species (sub-triangles 1 through 9 in Fig. S4, range size > 0.25 of the unit domain) and for smaller-ranged species (sub-triangles 10 through 16, range size ≤ 0.25 of the unit domain).

Midpoint predictor models

Midpoint predictor Model 1 does not constrain where range midpoints can occur within the domain, based on range size, but some locations are more probable than others based on measured environmental variables such as temperature or precipitation. Midpoint predictor Model 2 is the same as Model 1, except that it imposes geometric constraints, restricting the placement of the midpoint of each species (drawn from the empirical RSFD, without replacement) so that its range limits lie within the domain.

For both models, we assessed each of the same environmental variables used to interpret modeled attractors in the Bayesian model (Table S1), one variable at a time. The [0,1] domain was divided into 1000 bins, and we used a linear interpolation of environmental variables measured at different transect locations to fill each bin with an approximate value for the variable. Next, probabilities for each bin were assigned proportional to these measured values. Finally, a range midpoint representing each empirical species was placed stochastically in the domain in proportion to these values.

Midpoint predictor model evaluation. For each midpoint predictor model, we calculated the cumulative distribution function (cdf) of species range midpoints across the domain, averaged over 1000 simulations. Steeply rising sections of this cdf indicate elevations with a high concentration of species range midpoints, whereas flatter sections

of the cdf indicate elevations where few or no species range midpoints occur. We refer to this averaged cdf as the *model reference cdf*.

We next constructed the cdf for the empirical midpoint data and calculated the maximum difference between this curve and the model reference cdf. This difference is the traditional Kolmogorov-Smirnov test statistic. To generate a null distribution and estimate the tail probability for the empirical data, we generated 1000 additional midpoint distributions with the midpoint predictor model, and for each of these we calculated the K-S test statistic between the cdf of the single simulated midpoint distribution and the model reference cdf.

We then compared the histogram of the 1000 simulated K-S differences with the observed K-S difference between the empirical data and the model reference cdf. A non-significant one-tailed value ($P > 0.05$) indicates an adequate fit with the data. In contrast, unusually large K-S values for the observed data would suggest that the midpoint predictor model does not successfully reproduce the pattern of midpoints in the data.

Software

The midpoint predictor models were programmed in R version 3.1.1 (Team 2014), with base functions from the EcoSimR development package (https://github.com/GotelliLab/EcoSimR), which is available now as an R package. R scripts for the midpoint predictor model analyses and for plotting the graphics in Figs. 2, 3, and 4) are available from the authors. The midpoint attractor simulator and the MCMC sampler were implemented in 4th Dimension, in an extension of the RangeModel application (Colwell 2008) that is available from the authors.

SUPPLEMENTAL RESULTS

Midpoint attractors and geometric constraints

We expected (see *Main Text, Materials and Methods*) that empirical species richness would correlate more strongly with modeled species richness, as simulated by the midpoint attractor model, than with the attractor itself. This expectation was borne out in 12 of the 16 datasets (Table S3 and Fig. S1, *first and second panels for each dataset*). Among the four exceptions, in three cases (Costa Rican mammals, Australian moths, and Bornean geometrid moths) the fit of empirical richness to modeled richness does not differ, by AIC, from the fit of empirical richness to the attractor, and in three cases (Costa Rican mammals, Australian moths, and Australian parasitoids) the empirical richness pattern and modeled attractor were both centered near the middle of the elevational domain. As we discuss later (see *Supplemental Discussion*), with a centered attractor, we should not expect a consistent difference between modeled richness and the attractor in explaining empirical richness.

SUPPLEMENTAL DISCUSSION

The success of the simple, two-parameter Bayesian midpoint attractor model varied among datasets (Figs. 2, 3, and 4; Tables S2 and S3). Overall, however, the simulated richness patterns provided a good fit to the empirical data, regardless of the location of the attractor or the characteristics of the RSFD. Results of independent tests of modeled versus empirical midpoint density suggested that both small-ranged and large-ranged species respond to the same environmental gradients. Moreover, the mid-domain shift of mean midpoint locations for ranges on gradients with off-center attractors (Fig. 5) perhaps reconciles our results with the finding of some previous studies that species

richness for small- and large-ranged species is correlated with different environmental factors (Dunn *et al.* 2006). With off-center attractors, the increasing discordance between attractor and range midpoint for larger ranges (e.g. Bornean geometrid moths, Fig. 4) suggests that peaks of population density or other indicators of performance or fitness may lie closer to the attractor than to geometric range midpoints—a promising avenue for future research.

For nearly all datasets (14 of 16; all except Costa Rican ferns and N. American butterflies), even those that had several empirical richness points outside the 95% confidence interval envelope for the modeled data (Figs. 2, 3, and 4), the model produced a highly significant fit (median $P < 0.0001$) between the midpoint density of the empirical and modeled data, as assessed for the 16 smaller triangles within the constraint triangle (*right panels* in Figs. 2, 3, and 4). For a few datasets, a single attractor may not be an appropriate model. Bornean geometrid moths and perhaps North American mammals (Fig. 4) show signs of multimodal attractors, although the fit for a simple, unimodal attractor is nonetheless significant.

We emphasize that the *P*-values for correspondence between modeled and empirical point densities in the constraint triangle (Table S2) (including the large- *vs.* small-range analyses) represent an independent statistical assessment of the midpoint attractor simulations; they were not used in any way to select the best parameters for the midpoint attractor. Although a particular pattern of midpoint-range points in such a plot fully determines a corresponding pattern of species richness, the reverse is not true: similar richness patterns can arise from alternative placement of ranges within the

domain. However, there are constraints on the ways that a given set of ranges can be shuffled to approximate a given pattern of richness.

The case of centered midpoint attractors. When the best-fit attractor lies near the center of the domain, as it does for the Costa Rican ferns (Fig. 2) or North American butterflies (Fig. 4, Table S2), the modeled pattern of richness may be quite symmetrical—but so is the expected pattern from a simple MDE model of geometric constraints with no environmental drivers. For Costa Rican ferns, for example, the prediction of the MDE model differs little from the corresponding plot with an optimized midpoint attractor (Fig. S2). The sub-triangle statistical test for the Costa Rican ferns and North American butterfly datasets yields no evidence of an attractor ($P > 0.994$) (Table S2), nor do the tests for large and small ranges for these two datasets ($P > 0.983$). Although the modeled and empirical midpoint densities correspond closely in these two datasets, neither differs from a random distribution of midpoints (given the empirical RSFD), which is necessarily the baseline for judging significance (*SI Materials and Methods*). Costa Rican geometrid moths show this same result for small-ranged species.

In such cases, the most conservative conclusion is that we cannot distinguish between pure geometric constraints or a broad (but not too broad) environmental attractor with a peak near the center of the domain. Although the pure geometric constraints model has two fewer parameters and would thus be favored in a strict model selection approach, it seems more parsimonious, overall, to adopt a single model of interaction between attractor and constraints for all datasets. Other datasets with attractors closely centered on the domain (e.g. Costa Rican geometrid moths, for large ranges, Fig. 2, or Australian

moths or leaf-miner parasitoids, Fig. 4) differ from random midpoint locations enough that the test picks up the close correspondence between model and data (Table S2).

The failure of the midpoint predictor models. How can we reconcile failure of the midpoint predictor models with the success of the Bayesian midpoint attractor models? At least three, non-exclusive explanations are possible. First, we might have used the "wrong" environmental variables. Whereas the midpoint attractors, together with geometric constraints, produced a good fit to empirical species richness, the fit of the attractors themselves to environmental variables was often rather poor (Table S3; third and fourth panel in each graph in Fig. S1). The original investigators for our datasets measured important aspects of temperature, precipitation, and other variables (such as plant cover) that are thought to affect species richness on elevational gradients. Primary productivity is thought to be a key correlate of species richness for many groups (Storch *et al.* 2006). However, primary productivity is difficult to measure directly, it cannot currently be estimated accurately on small spatial scales from remotely sensed data, and is missing from all our datasets.

Second, we might have analyzed the right variables, but we had the wrong functional form (linear) for a more complex relationship between the probability of midpoint occurrence and measured conditions. In preliminary analyses, however, alternative functional forms (e.g., logarithmic, exponential) did not improve the fit. For many of our datasets, such as Bornean geometrid moths and New Guinean butterflies, the high concentration of species range midpoints in the lower elevations of the domain cannot be accounted for by any univariate or multivariate transformation of the available environmental variables.

A third possibility is a history of strong niche conservatism (Graham *et al.* 2014; Wu *et al.* 2014), in which large clades evolved and diversified within a climatic zone (around a midpoint attractor) but did not diverge, among themselves, in relation to environmental gradients within that zone. Concentrations of elevational range midpoints may arise from rapid, clade-based "colonization" of new midpoint attractors (e.g., transitions from lowland to montane specialists) followed by net diversification. A search for multimodal attractors and alignment with phylogenetic structure would be a fruitful area of future research.

Appendix 2: Supplemental Tables and Figures

Supplemental Tables

Table S1. The datasets and their characteristics. *Sampling limits* represent the lowest and highest occurrence on a unit-line transect, after range adjustments described in the *Suplemental Materials and Methods* (Dataset Selection and Preparation). *Sampling scope* is the difference between the sampling limits.

Dataset	Locality	Transect coordinates	vationsSampling	Sampling limits	Sampling scope	s))Domain limits	Sampling method	Species	Environmental variables and their units	Data provider	Collection dates	Published references to the dataset
Costa Rica Datasets												
Ants	Barva Transect (Prov. Heredia)	10°08'N–10°26'N, 84°00'W–84°07'W	7	0.004, 0.705	0.701	0, 2900	Miniwinkler extractors	332	MAT (°C), Mean RH (%), MAP (mm), Area (% of total per 100m band)	John T. Longino	2001-2007	(Longino & Colwell 2011; Longino *et al.* 2014)
Arctiine moths	Barva Transect (Prov. Heredia)	10°08'N–10°26'N, 84°00'W–84°07'W	12	0.013, 0.940	0.927	0, 2900	Light traps, manual collection	222	MAT (°C), Mean RH (%), MAP (mm), Area (% of total per 100m band)	Gunnar Brehm	2003–2004	None

Dataset	Locality	Transect coordinates	vationsSampling	Sampling limits	Sampling scope	s))Domain limits	Sampling method	Species	Environmental variables and their units	Data provider	Collection dates	Published references to the dataset
Geometrid moths	Barva Transect (Prov. Heredia)	10°08'N–10°26'N, 84°00'W–84°07'W	12	0.013, 0.940	0.927	0, 2900	Light traps, manual collection	739	MAT (°C), Mean RH (%), MAP (mm), Area (% of total per 100m band)	Gunnar Brehm	2003–2004	(Brehm *et al.* 2007)
Ferns	Barva Transect (Prov. Heredia)	10°08'N–10°26'N, 84°00'W–84°07'W	29	0.011, 0.986	0.975	0, 2900	Plot-based (20x20m²)	434	MAT (°C), Mean RH (%), MAP (mm), Area (% of total per 100m band)	Jürgen Kluge	2002-2003	(Kluge *et al.* 2006)
Mammals	Tilarán Mt. Range	10°23'N–10°17'N, 84°47'W–84°26'W	18	0.000, 0.998	0.989	0, 1840	Live traps, kill traps, and pitfall traps	18	Average Temperature (°C), Annual Precipitation (mm) [worldclim], elevational area (km2 per 100m elevational band) [DEM, ArcGIS]	Christy McCain	2000-2002	(McCain 2004; McCain 2005)
Papua New Guinea Datasets												
Ants	Mt. Wilhelm Transect	5°44'S–5°47'S, 145°03'E–145°20'E	8	0.007, 0.822	0.815	0, 4509	Pitfall trapping and hand-collecting Yusah et al. (2012))	118	MAT (°C), Mean RH (%), MAP (mm), Area (% of total per 100m band)	Jimmy Moses, Tom M. Fayle, Petr Klimes	2012	(Moses 2015)

150

Dataset	Locality	Transect coordinates	vationsSampling	Sampling limits	Sampling scope	s))Domain limits	Sampling method	Species	Environmental variables and their units	Data provider	Collection dates	Published references to the dataset
Butterflies	Mt. Wilhelm Transect	5°44'S–5°47'S, 145°03'E–145°20'E	8	0.022, 0.876	0.854	0, 4509	Modified Pollard transects (Caldas & Robbins 2003)	264	MAT (°C), Mean RH (%), MAP (mm), Area (% of total per 100m band)	Legi Sam	2009	(Sam 2011)
Birds	Mt. Wilhelm Transect	5°44'S–5°47'S, 145°03'E–145°20'E	8	0.022, 0.876	0.854	0, 4509	Point-counts, mist-netting	245	MAT (°C), Mean RH (%), Mean Tree Height (m), Mean Tree Basal Area (cm2)	Katerina Sam	2010-2012	(Tvardikova 2013; Sam & Koane 2014)
Ferns	Mt. Wilhelm Transect	5°44'S–5°47vS, 145°03'E–145°20'E	8	0.022, 0.876	0.854	0, 4509	Plot-based (20x20m²)	359	MAT (°C), Mean RH (%), MAP (mm), Area (% of total per 100m band)	D.N. Karger, S. Noben, M. Lehnert, M.S. Sundue	2014	None
Australia Datasets												
Moths (macromoths + Pyraloidea)	Border Ranges (NSW)	28°24'S–28°22'S, 153°1'E–153°5'E	5	0.220, 0.959	0.739	0, 1100	Light traps	612	°C min, max median, average plant richness	Louise Ashton, Roger Kitching	2009-2010	(Ashton *et al.* In press.)

Dataset	Locality	Transect coordinates	vationsSampling	Sampling limits	Sampling scope	s)Domain limits	Sampling method	Species	Environmental variables and their units	Data provider	Collection dates	Published references to the dataset
Leaf miners (Lepidoptera, Coleoptera, Diptera, Hymenoptera)	Border Ranges (NSW)	28°24'S–28°22'S, 153°1'E–153°5'E	5	0.183, 0.981	0.798	0, 1100	Hand collecting and rearing	34	Average Temperature (°C), Annual Precipitation (mm), Vegetation cover (log of cm's intercepted)	Sarah Maunsell	2011 - 2012	(Maunsell *et al.* In press.)
Leaf miner parasitoids (Hymenoptera)	Border Ranges (NSW)	28°24'S–28°22'S, 153°1'E–153°5'E	5	0.183, 0.981	0.798	0, 1100	Hand collecting and rearing	14	Average Temperature (°C), Annual Precipitation (mm), Vegetation cover (log of cm's intercepted)	Sarah Maunsell	2011 - 2012	(Maunsell *et al.* 2015)
Borneo Datasets												
Geometrid moths	NE Borneo	1°28'N-6°16'N, 112°06'E-117°53'E	70	0.000, 0.958	0.958	0, 4095	Light traps	775	Average Temperature (°C), Annual Precipitation (mm) [worldclim], forest stratum, vegetation type [field descriptions]	Jan Beck, Jeremy Hollo-way, Chey Vun Khen	1965-2003	(Beck *et al.* 2012) (undis-turbed habitats only)
Sphingid moths	NE Borneo	0°05'S-6°18'N, 109°43'E-118°10'E	19	0.000, 0.958	0.958	0, 4095	Light traps	102	Average Temperature (°C), Annual Precipitation	Jan Beck, Ian Kitching et al.	1965-2005	(Beck & Kitching 2009)

Dataset	Locality	Transect coordinates	vationsSampling	Sampling limits	Sampling scope	s))Domain limits	Sampling method	Species	Environmental variables and their units	Data provider	Collection dates	Published references to the dataset
									(mm) [worldclim], area [of 200m bands], vegetation type [globcov]			
North America Datasets												
Butterflies	Califor-nia	38°34'N-39°20'N, 120°20'-121°25'W	6	0.001, 0.966	0.965	0, 2775	Pollard walk, presence/ absence	129	Average Max Daily Temperature (°C), Average Min Daily Temperature (°C), Annual Precipitation (mm)	Arthur Shapiro	1973-2014	(Forister *et al.* 2010).
Mammals	Yosemite NP (Califor-nia)	37°30'N–37°59'N, 118°56'–120°28'W	40	0.000, 0.990	0.990	0, 3997	Live traps, kill traps, hunting, visual observations	46	Average Temperature (°C), Annual Precipitation (mm) [worldclim], elevational area (km per 100m elevational band) [DEM, ArcGIS]	Joseph Grinnell & Tracy Storer	1914-1916, 1919.	(Grinnell & Storer 1924; McCain 2005)

1041
1042

159

Table S2. Midpoint attractors. The correspondence between midpoint density arising from the midpoint attractor model and the corresponding observed midpoint density was tested for significance for all ranges, for large ranges (≥ 0.25 of the unit domain), and for small ranges (< 0.25 of the unit domain). Insignificant tests are reported in boldfaced italics.

	Attractor Mean	Attractor SD	Mean midpoint	Mean range	R^2 all ranges	P all ranges	R^2 large ranges	P large ranges	R^2 small ranges	P small ranges
Costa Rica Datasets										
Ants	0.065	0.023	0.196	0.181	0.949	0.001	0.968	0.001	0.955	0.001
Arctiine moths	0.378	0.294	0.332	0.228	0.770	0.001	0.747	0.001	0.768	0.001
Geometrid moths	0.527	0.327	0.492	0.306	0.650	0.002	0.762	0.001	***0.155***	***0.999***
Ferns	0.473	0.331	0.479	0.303	***0.466***	***0.999***	***0.617***	***0.997***	***0.368***	***0.999***
Mammals	0.604	0.401	0.521	0.425	0.675	0.001	0.744	0.001	0.007	0.001
Papua New Guinea Datasets										
Ants	0.153	0.123	0.199	0.156	0.867	0.001	0.995	0.001	0.832	0.001
Butterflies	0.098	0.239	0.205	0.180	0.954	0.001	0.998	0.001	0.941	0.001
Birds	0.243	0.411	0.330	0.285	0.918	0.001	0.899	0.001	0.968	0.001
Ferns	0.440	0.222	0.447	0.156	0.801	0.001	0.548	0.001	0.246	0.001
Australia Border Ranges Datasets										
Moths	0.555	0.291	0.583	0.419	0.912	0.001	0.939	0.001	0.831	0.001
Leaf miners	0.742	0.418	0.630	0.426	0.555	0.015	0.542	0.013	***0.569***	***0.999***
Leaf-miner parasitoids	0.492	0.219	0.534	0.493	0.551	0.003	0.553	0.003	***0.436***	***0.758***
Borneo Datasets										
Geometrid moths	0.151	0.181	0.226	0.173	0.840	0.001	0.626	0.001	0.868	0.001
Sphingid moths	0.104	0.120	0.214	0.342	0.993	0.001	1.000	0.001	0.966	0.001
North America Datasets										

Butterflies	0.532	0.476	0.502	0.486	***0.632***	***0.996***	***0.635***	***0.997***	***0.448***	***0.983***
Mammals	0.435	0.282	0.381	0.353	0.435	0.001	0.371	0.009	0.724	0.001

Table S3. Midpoint attractors in relation to environmental variables and observed species richness, analyzed by multiple regression with AIC-based model selection. Values of $R^2 < 0.5$ are set in italics. Values of delta AIC > 3 are boldfaced. The corresponding scatterplots appear in Fig. S1. Because the attractor is a continuous function (a doubly-truncated Gaussian distribution) and the other variables are spatially autocorrelated, significance probabilities cannot be assigned to R^2 values, which are thus best viewed as comparative.

Dataset	**Response Variable**	**Predictor Variables**	***n***	***R*²**	**Condition Number**	**Delta AIC**
Costa Rica Datasets						
Ants	Empirical richness	Temperature	10	0.856	1.000	0.000
	Attractor	Temperature & Relative humidity	10	0.971	2.354	0.000
		Temperature & Area	10	0.971	4.625	1.332
		Temperature & Precipitation	10	0.972	2.548	1.857
	Empirical richness	Modeled richness	10	0.942	1.000	0.000
		Attractor	10	0.845	1.000	**9.563**
Arctiine moths	Empirical richness	Temperature & Area	10	0.927	4.625	0.000
		Precipitation	10	0.839	1.000	1.896
	Attractor	Precipitation & Area	10	0.852	1.616	0.000
		Relative humidity & Precipitation	10	0.833	1.040	1.217
		Temperature & Precipitation	10	0.825	2.548	1.712
		Precipitation	10	0.678	1.000	1.793
	Empirical richness	Modeled richness	10	0.879	1.000	0.000
		Attractor	10	0.762	1.000	**6.770**

Dataset	**Response Variable**	**Predictor Variables**	***n***	***R^2***	**Condition Number**	**Delta AIC**
Geometrid moths	Empirical	Area	10	0.647	1.000	0.000
		Temperature & Area	10	0.788	4.625	0.899
		Relative humidity	10	0.608	1.000	1.037
		Precipitation & Area	10	0.744	1.616	2.377
	Attractor	Relative humidity		0.623	1.000	0.000
	Empirical richness	Modeled richness	10	0.898	1.000	0.000
		Attractor	10	0.869	1.000	2.448
Ferns	Empirical richness	Precipitation & Area	10	0.785	1.616	0.000
		Temperature & Area	10	0.770	4.625	0.690
		Relative humidity	10	0.560	1.000	1.165
	Attractor	Relative humidity	10	0.666	1.000	0.000
	Empirical richness	Modeled richness	10	0.898	1.000	0.000
		Attractor	10	0.883	1.000	1.312
Mammals	Empirical richness	Area	10	*0.043*	1.000	0.000
		Precipitation	10	*0.020*	1.000	0.267
		Temperature	10	*0.013*	1.000	0.348
	Attractor	Area	10	*0.483*	1.000	0.000
	Empirical richness	Attractor	10	0.630	1.000	0.000
		Modeled richness	10	0.611	1.000	0.538
Papua New Guinea Datasets						
Ants	Empirical richness	Temperature	8	0.867	1.000	0.000
	Attractor	Temperature	8	0.586	1.000	0.000
		Tree height	8	0.539	1.000	0.859
	Empirical richness	Modeled richness	8	0.894	1.000	0.000
		Attractor	8	0.861	1.000	2.142

Dataset	**Response Variable**	**Predictor Variables**	***n***	***R^2***	**Condition Number**	**Delta AIC**
Butterflies	Empirical richness	Temperature	8	0.842	1.000	0.000
	Attractor	Temperature	8	0.925	1.000	0.000
		Temperature & Relative humidity	8	0.968	1.812	2.486
	Empirical richness	Modeled richness	8	0.975	1.000	0.000
		Attractor	8	0.950	1.000	**5.461**
Birds	Empirical richness	Temperature	8	0.958	1.000	0.000
		Temperature & Basal area	8	0.985	1.360	1.299
	Attractor	Temperature	8	0.804	1.000	0.000
		Tree height	8	0.731	1.000	2.530
	Empirical richness	Modeled richness	8	0.935	1.000	0.000
		Attractor	8	0.876	1.000	**5.222**
Ferns	Empirical richness	Basal area	8	*0.442*	1.000	0.000
		Humidity	8	*0.236*	1.000	2.518
	Attractor	Basal area	8	*0.447*	1.000	0.000
		Humidity	8	*0.272*	1.000	2.207
	Empirical richness	Modeled richness	8	0.813	1.000	0.000
		Attractor	8	0.810	1.000	0.137
Australia Datasets						
Moths*	Empirical richness	Temperature-Precipitation PCA	10	*0.123*	1.000	0.000
		Tree Richness	10	*0.122*	1.000	0.007
	Attractor	Temperature-Precipitation PCA	10	*0.139*	1.000	0.000
		Tree Richness	10	*0.078*	1.000	0.625
	Empirical richness	Attractor	10	0.926	1.000	0.000
		Modeled richness	10	0.907	1.000	1.966
Leaf-miners	Empirical richness	Temperature-Precipitation PCA & Tree richness	10	0.704	1.357	0.000

Dataset	Response Variable	Predictor Variables	*n*	R^2	Condition Number	Delta AIC
		Tree Richness	10	*0.338*	1.000	0.032
		Temperature-Precipitation PCA	10	*0.164*	1.000	2.131
	Attractor	Temperature-Precipitation PCA	10	0.560	1.000	0.000
	Empirical richness	Modeled richness	10	*0.342*	1.000	1.000
		Attractor	10	*0.163*	1.000	2.162
Leaf-miner parasitoids	Empirical richness	Temperature-Precipitation PCA	10	*0.476*	1.000	0.000
	Attractor	Temperature-Precipitation PCA	10	*0.442*	0.939	0.000
	Empirical richness	Attractor	10	0.939	1.000	0.000
		Modeled richness	10	0.770	1.000	**11.878**
Borneo Datasets						
Geometrid Moths	Empirical richness	Temperature	10	*0.188*	1.000	0.000
		Precipitation	10	*0.068*	1.000	1.337
	Attractor	Temperature	10	0.680	1.000	0.000
	Empirical richness	Attractor	10	*0.469*	1.000	0.000
		Modeled richness	10	*0.461*	1.000	0.152
Sphingid moths	Empirical richness	Temperature & Area	10	0.944	2.034	0.000
	Attractor	Temperature	10	0.702	1.000	0.000
		Cover Classes	10	0.683	1.000	0.614
	Empirical richness	Modeled richness	10	0.994	1.000	0.000
		Attractor	10	0.713	1.000	**38.012**
North American Datasets						
Butterflies	Empirical richness	Precipitation	11	0.533	1.000	0.000
	Attractor	Precipitation	11	*0.404*	1.000	0.000
		Precipitation & Minimum temperature	11	0.624	2.324	0.170

Dataset	**Response Variable**	**Predictor Variables**	***n***	***R*²**	**Condition Number**	**Delta AIC**
		Precipitation & Maximum temperature	11	0.590	2.265	1.120
	Empirical richness	Modeled richness	11	0.968	1.000	0.000
		Attractor	11	0.936	1.000	**7.506**
Mammals	Empirical richness	Precipitation	10	*0.154*	1.000	0.000
		Area	10	*0.140*	1.000	0.163
		Temperature	10	*0.034*	1.000	1.327
	Attractor	Precipitation	10	*0.429*	1.000	0.000
	Empirical richness	Modeled richness	10	0.725	1.000	0.000
		Attractor	10	0.697	1.000	**4.655**

*Temperature and precipitation were highly (inversely) correlated for the Australian moths dataset (Condition Number = 21.696). PCA was extracted to reduce the effects of collinearity.

Table S4. Analysis of midpoint predictor models for range midpoint locations. Each row represents a different environmental variable that was used to model probabilities of midpoint occurrence along the domain. A plus sign (+) indicates $P < 0.05$, meaning that the results were improbable relative to a particular model ($P(data|model)$). Numerical entries indicate one-tailed P values, based on 1000 simulations, for which $P > 0.05$ indicates that the data were not improbable, given the model. See *Supplemental Materials and Methods* for the algorithms of the two midpoint predictor models.

Dataset	Environmental Variable	Model 1	Model 2
Costa Rica Datasets			
Ants	Temperature	+	+
	Precipitation	+	+
	Relative humidity	+	+
	Area	+	+
Arctiine moths	Temperature	+	+
	Precipitation	+	+
	Relative humidity	+	+
	Area	+	+
Geometrid moths	Temperature	+	+
	Precipitation	+	+
	Relative humidity	+	+
	Area	+	+
Ferns	Temperature	+	+
	Precipitation	+	+
	Relative humidity	+	+
	Area	+	+
Mammals	Temperature	0.277	0.294
	Precipitation	0.300	0.305
	Area	+	+
Papua New Guinea Datasets			
Ants	Temperature	+	+
	Relative humidity	+	+
	Tree height	+	+
	Basal area	+	+
Butterflies	Temperature	+	+
	Relative humidity	+	+

Dataset	Environmental Variable	Model 1	Model 2
	Tree height	+	+
	Basal area	+	+
Birds	Temperature	+	+
	Relative humidity	+	+
	Tree height	+	+
	Basal area	+	+
Ferns	Temperature	+	+
	Relative humidity	+	+
	Tree height	+	+
	Basal area	+	+
Australia Datasets			
Moths	Temperature	+	+
	Precipitation	+	+
	Tree richness	+	+
Leaf-miners	Temperature	+	+
	Precipitation	0.132	0.083
	Tree richness	+	+
Leaf-miner parasitoids	Temperature	+	0.053
	Precipitation	+	0.056
	Tree richness	0.074	0.153
Borneo Datasets			
Geometrid moths	Temperature	+	+
	Precipitation	+	+
Sphingid moths	Temperature	+	+
	Precipitation	+	+
	Area	+	+
	Cover classes	+	+
North American Datasets			
Butterflies	Minimum temperature	+	+
	Maximum temperature	+	+
	Precipitation	+	+
Mammals	Temperature	0.266	0.069
	Precipitation	0.230	+
	Area	0.154	+

Supplemental Figure Captions

*(**Note:** In the all-in-one pdf prepared for peer review, each caption appears in context with the corresponding figure at the end of the file.)*

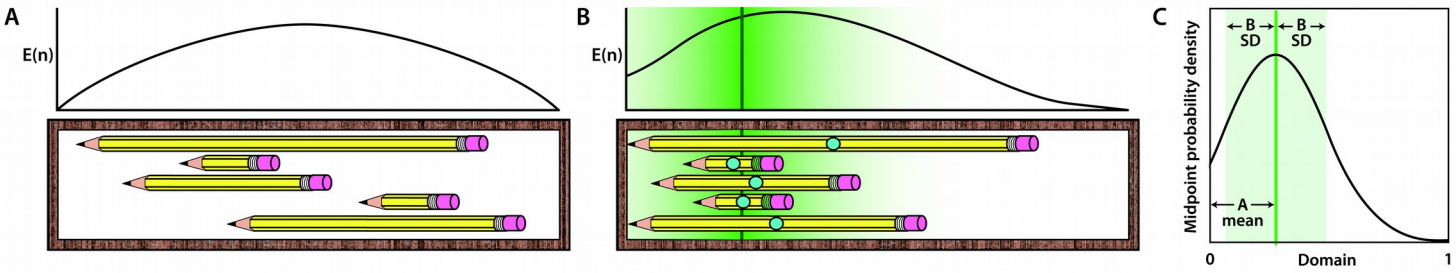

1073**Fig. 1.** Geometric constraint models. **(A)** The ***classic geometric constraint model***
1074illustrated by a physical analogy: a set of pencils (species), some shorter and some longer
1075(narrower and wider elevational ranges), stored in a schoolchild's old-fashioned pencil-
1076box (the bounded elevational domain) (Colwell *et al.* 2004). If the box is shaken end to
1077end, horizontally, so that the position of each pencil is randomized, the expected number
1078$E(n)$ of pencils that overlap (species richness) near the middle of the box is inevitably
1079greater than the number that overlap nearer the ends of the box, a pattern that is
1080symmetric around the center of the box. But the constraint does not act uniformly on the
1081pencils as the box is shaken: the shorter pencil stubs move more widely and freely than
1082the longer pencils. By analogy, the distribution of small-ranged species is less constrained
1083by geometry than the distribution of large-ranged species (Colwell & Lees 2000; Dunn *et*
1084*al.* 2007). **(B)** A physical analogy for the ***midpoint attractor model.*** Suppose that each
1085pencil has a steel ball bearing embedded at its midpoint (blue circles). A magnetic field,
1086the attractor, is applied across the pencil box (green). As the box is shaken end to end, the
1087pencils tend to collect near the attractor, as their midpoint ball bearings are drawn
1088towards the magnet. If the attractor is located near one end of the box, as illustrated, the
1089expected number of pencils $E(n)$ that stack up at any location along the length of the
1090pencil box is asymmetric. However, because the midpoints of the longer pencils cannot
1091align with the magnet (instead abutting the end of the box), the peak of $E(n)$ does not
1092coincide with the center of the attractor. Thus $E(n)$ is influenced jointly by the attractor
1093(the magnet) and the constraint (the limits of the pencil box). The pattern of $E(n)$ is
1094narrow when the attractor is strong, broad when the attractor is weak. **(C)** ***The midpoint***
1095***attractor*** modeled with a doubly-truncated Gaussian probability density function with
1096mean A and standard deviation B. Parameter A controls the position of the attractor on the

gradient. Parameter *B* controls the strength of the attractor (small *B* = a strong attractor, large *B* = a weak attractor).

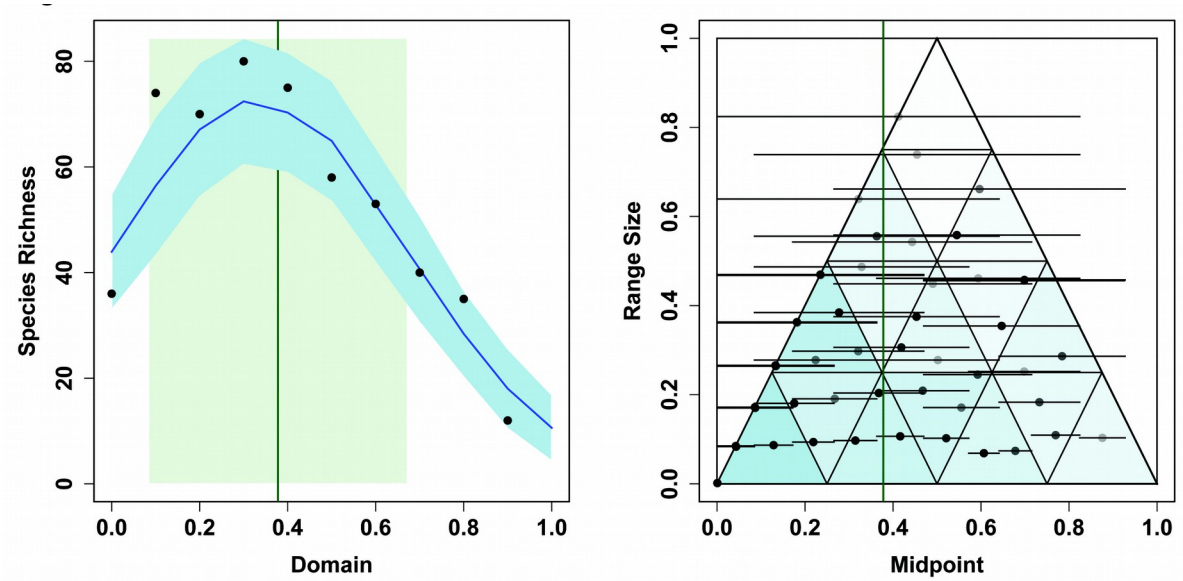

Fig. 2. The Bayesian midpoint attractor model applied to the Costa Rican arctiine moth dataset (222 species sampled across a 2906m elevational domain, rescaled to a [0,1] unit line). *Left panel*: Mean species richness (dark blue line) and 95% confidence interval (light blue band) for 100 simulations. The simulation is driven by a midpoint attractor (dark green vertical line) at 0.378, with a standard deviation (light green rectangle) of 0.294. These parameter values were chosen maximize the fit of modeled species richness (blue line) to empirical species richness pattern (black dots), using a simple MCMC Gibbs sampler. Empirical range sizes are maintained in the simulation. *Right panel:* Midpoint-range plot for the same data. The *x*-axis is the location of the range midpoint for each species on the elevational domain, and the *y*-axis plots the elevational span of the range (range size). The triangle sets the geometrically feasible midpoint limits for ranges of a given size. Black and grey points and associated horizontal line segments illustrate the empirical midpoint and range values for the 222 species of moths. Because many species have identical ranges and midpoints in this dataset, the shading of each point is proportional to the number of coincident species midpoints. The white-to-blue color scale in the 16 small triangles is proportional to the mean number of modeled points falling in

each triangle, averaged over the 100 runs of the simulation. The correspondence between the number of empirical points (black point density and color saturation) and the average number of modeled points (blue saturation) among the 16 small triangles is significant at $P < 0.001$ for this dataset (*Appendix 2*, Table S2). (See *Appendix 1, Supplemental Materials and Methods* for details of the test.)

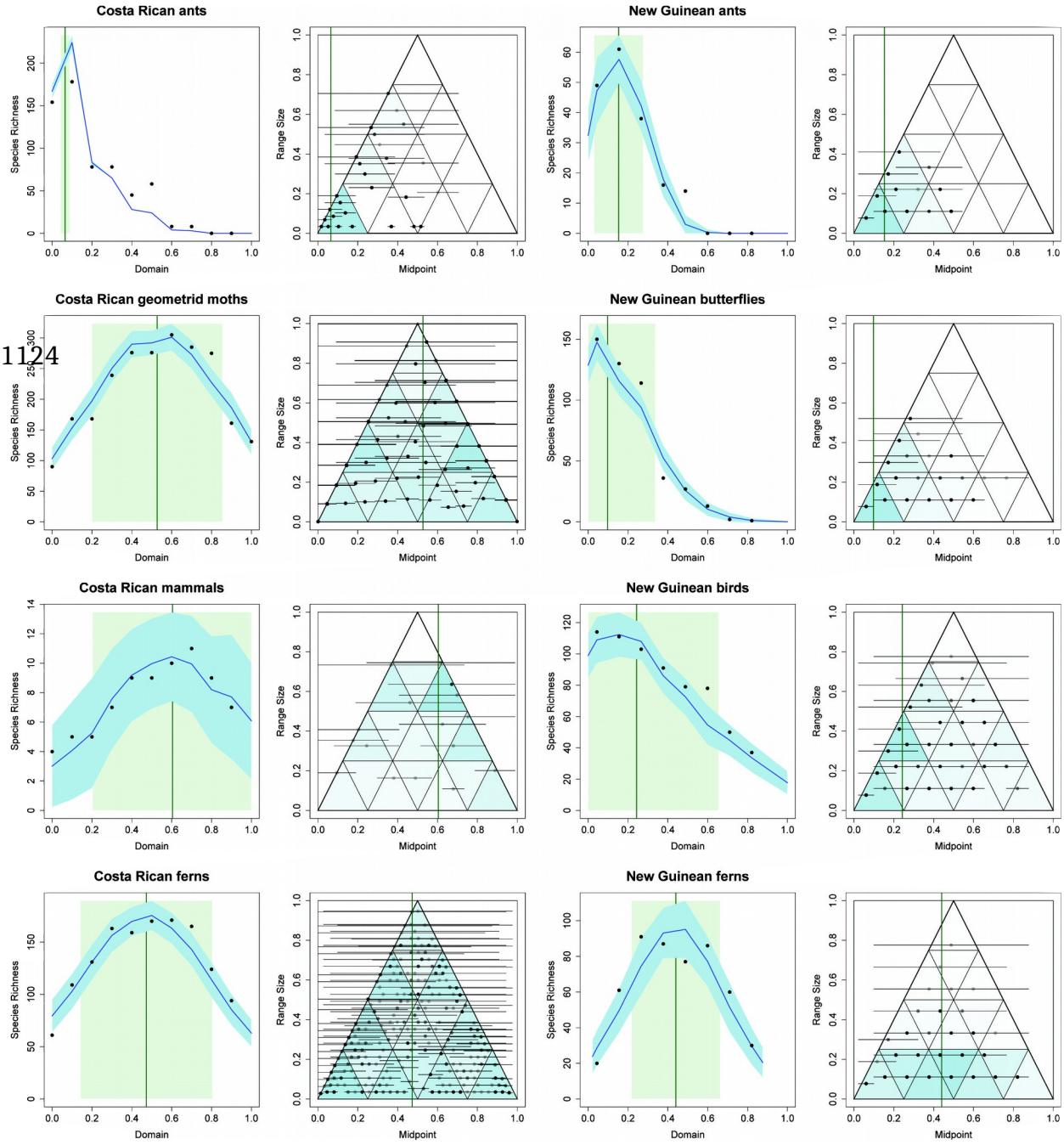

Fig. 3. The Bayesian midpoint attractor model applied to four datasets from the same elevational gradient (or, for mammals, a nearby gradient) in Costa Rica (*panel columns 1 and 2*) and four datasets from a single elevational gradient in Papua New Guinea (*panel columns 3 and 4*). The number of empirical points (black point density and color saturation) and the average number of modeled points (blue saturation) among the 16 small triangles is significant at $P < 0.001$ for 7 of the 8 datasets (Costa Rican ferns are the exception; see *Appendix 2, Supplemental Discussion* on centered attractors). A fifth dataset from the same Costa Rican gradient appears in Fig. 2, and Fig. 3 shows 7 additional datasets. See Fig. 2 for graphical details, *Appendix 2*, Table S2 for statistical results, and *Appendix 2*, Table S1 for details of the datasets.

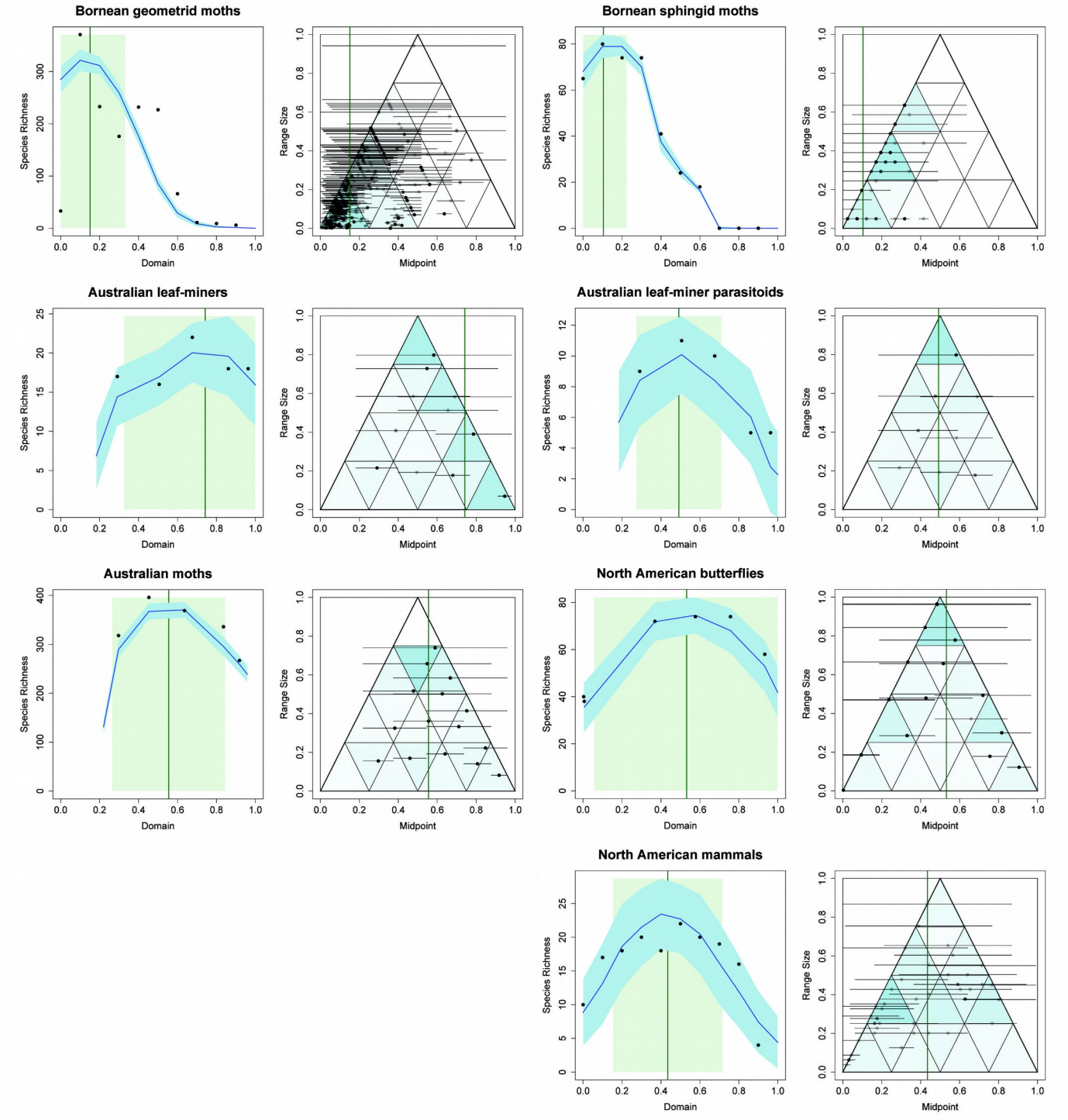

1137**Fig. 4.** The Bayesian midpoint attractor model applied to seven datasets from Borneo,
1138Australia, and North America. See Fig. 2 caption for graphical details, *Appendix 2* Table
1139S2 for statistical results, and *Appendix 2* Table S1 for details of the data sets.

1140

1141

1142**Fig. 5.** The signature of geometric constraints in the modeled patterns of species richness.

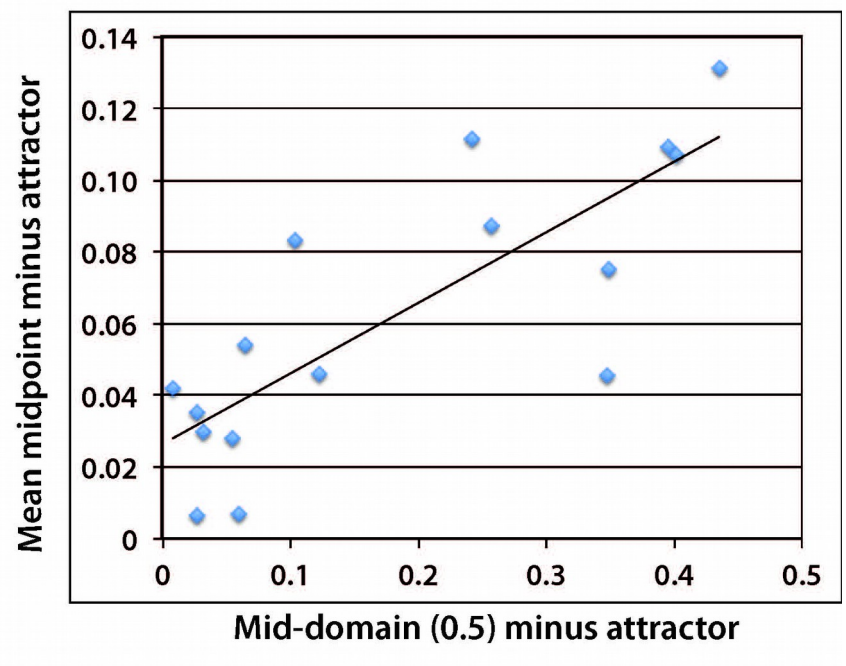

1143The closer the modeled attractor lies to a domain limit, the greater the discrepancy
1144between the location of the attractor and the mean location of range midpoints on the
1145domain. The graph shows the relationship between $|(mean\ midpoint - attractor)|$
1146and $|(0.5 - attractor)|$. Each point represents a different dataset (n = 16, *slope* = 0.592, P
1147< 0002). See Table S2 for data points.

1148

A

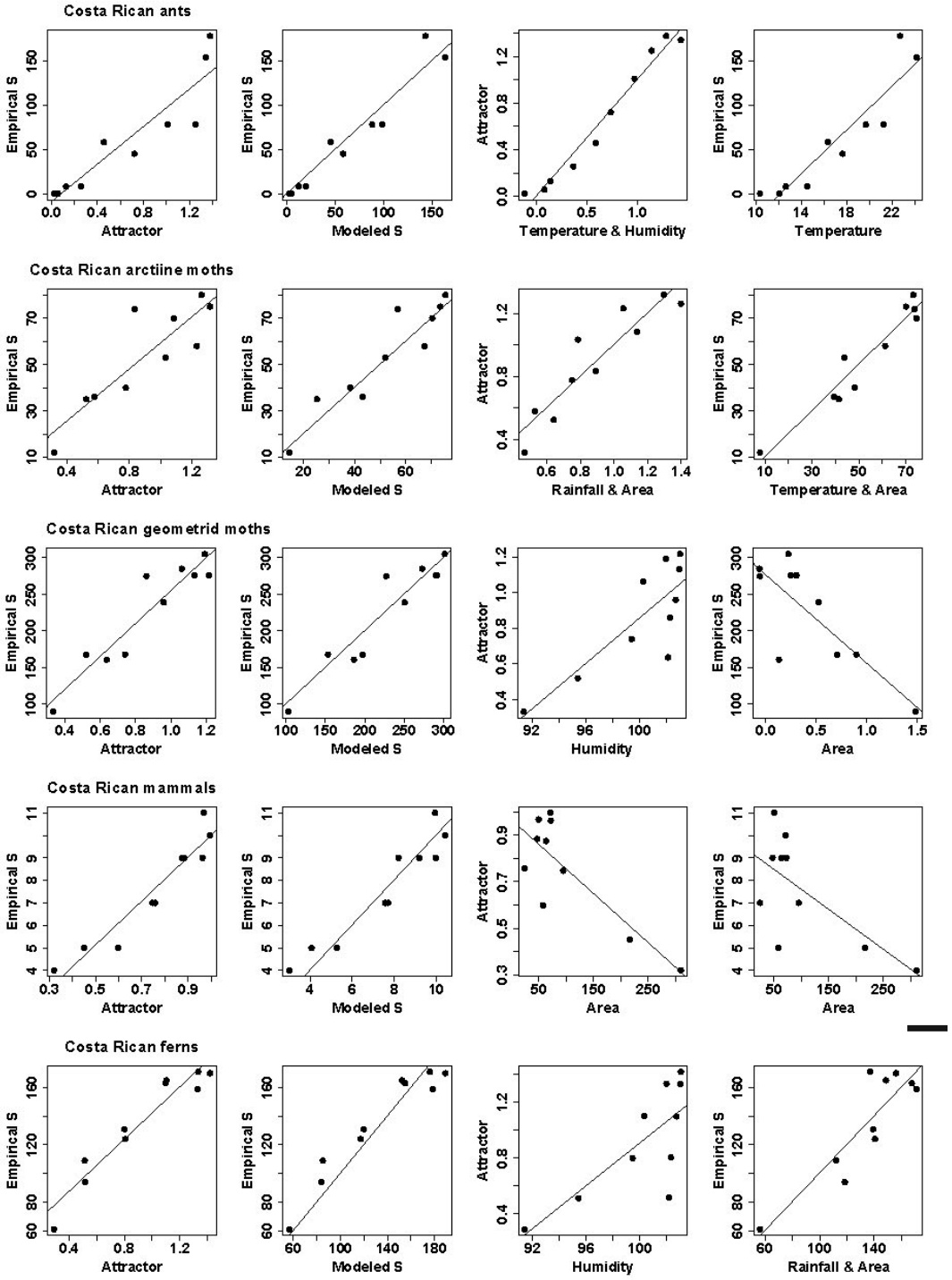
Costa Rican ants
Empirical S
Attractor
Modeled S
Temperature & Humidity
Temperature
Costa Rican arctiine moths
Rainfall & Area
Temperature & Area
Costa Rican geometrid moths
Humidity
Area
Costa Rican mammals
Costa Rican ferns
Rainfall & Area

1150

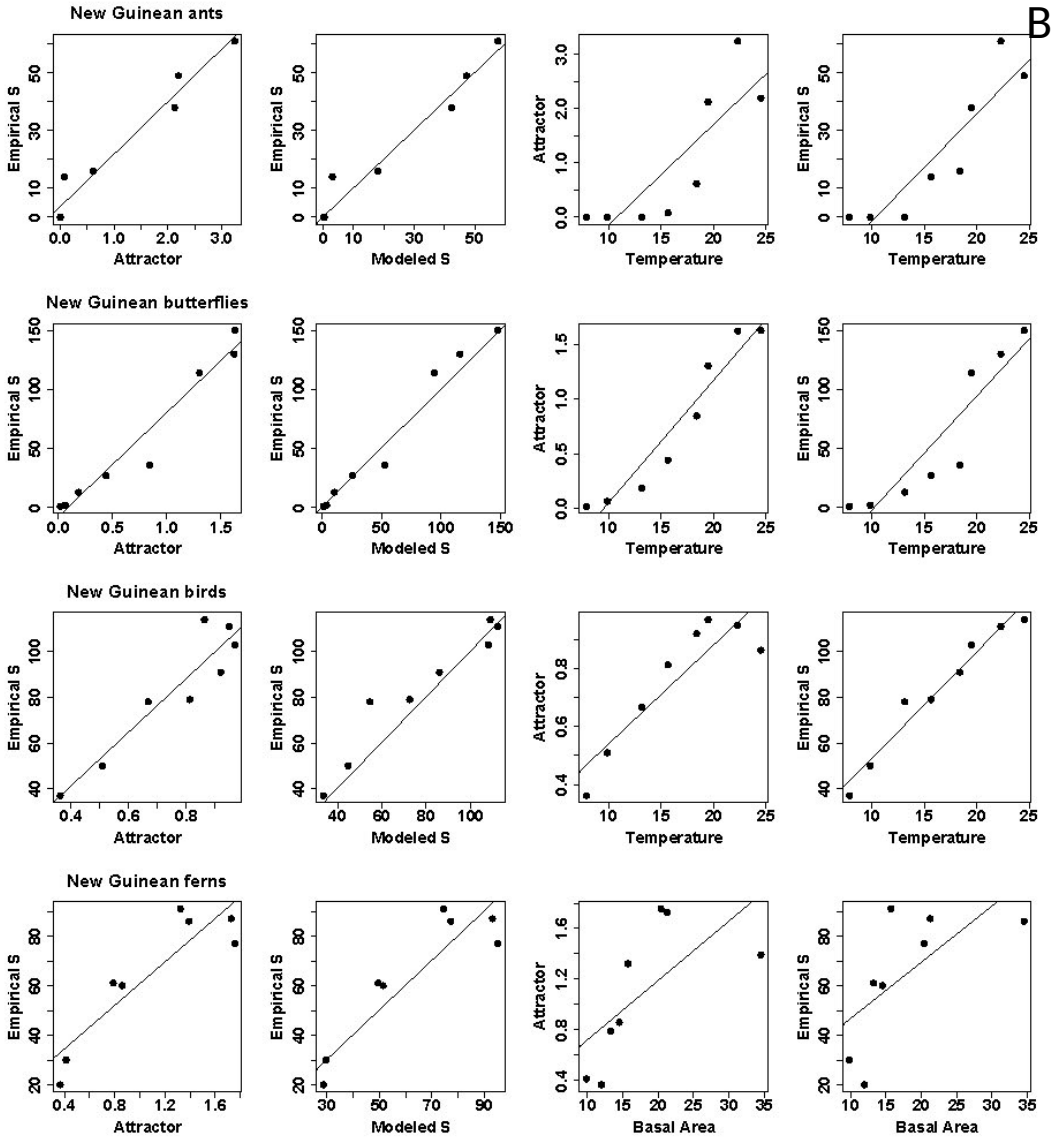
B
New Guinean ants
Empirical S
Attractor
Modeled S
Temperature
New Guinean butterflies
New Guinean birds
New Guinean ferns
Basal Area

1151

C

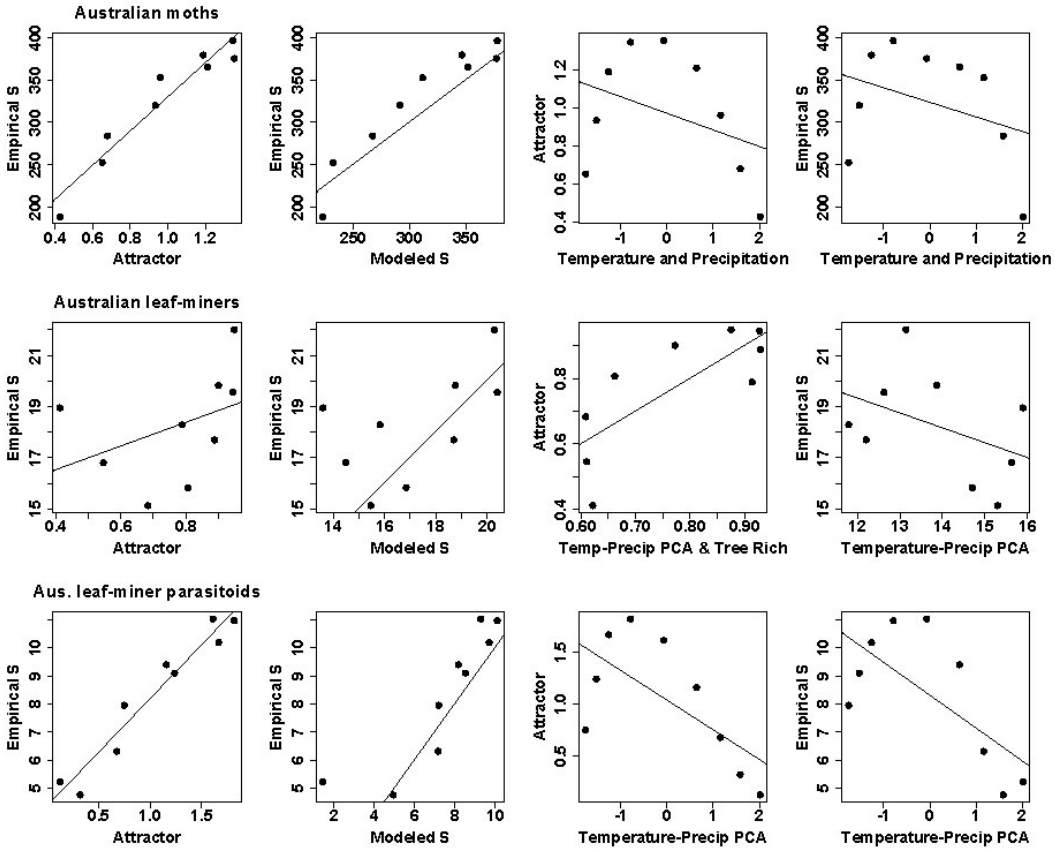
Australian moths
Empirical S
Attractor
Modeled S
Temperature and Precipitation
Australian leaf-miners
Temp-Precip PCA & Tree Rich
Temperature-Precip PCA
Aus. leaf-miner parasitoids

D

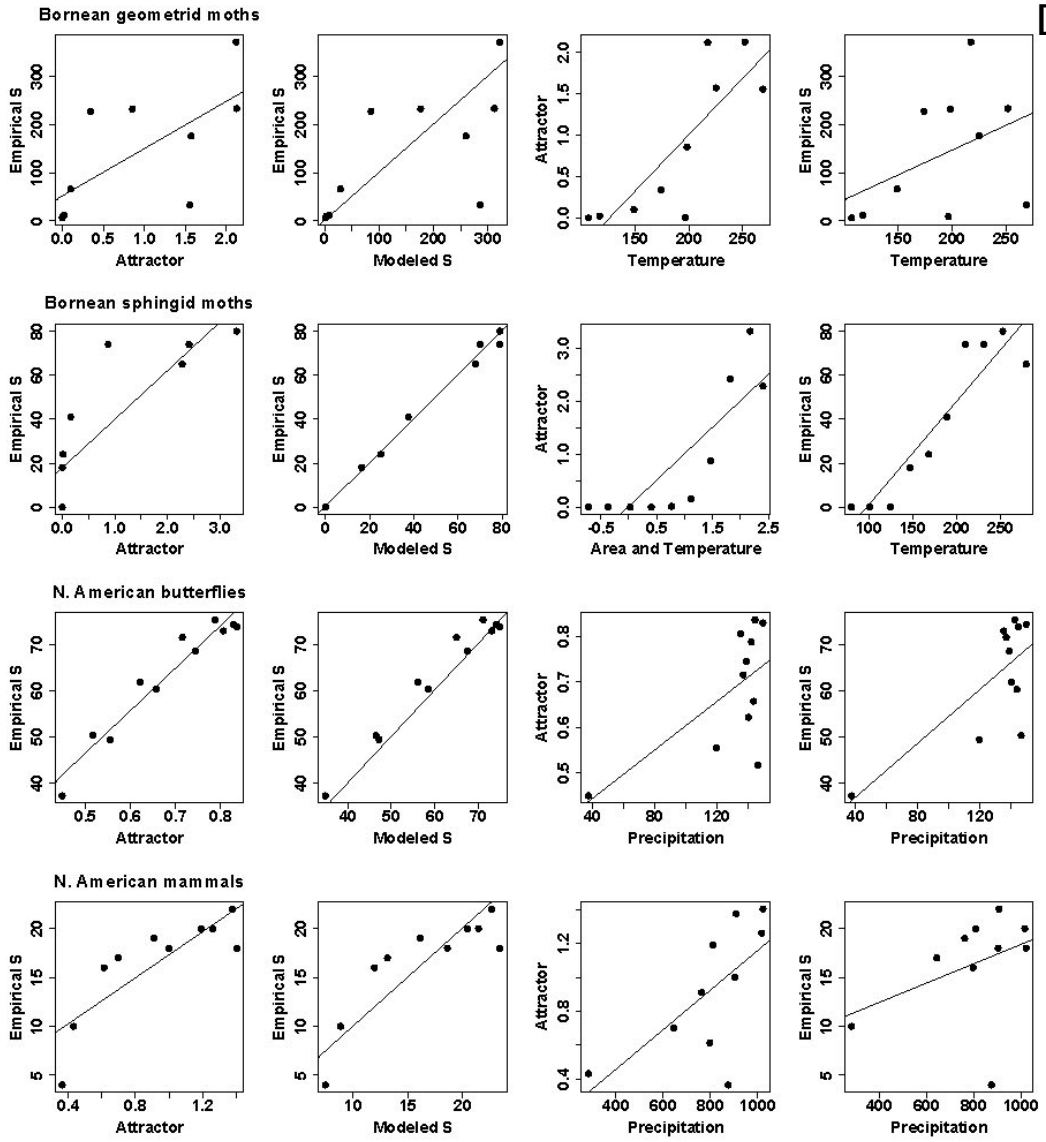

***Appendix 2*, Fig. S1, A-D.** Relationships between the modeled attractor, simulated species richness, empirical species richness, and measured environmental variables for each of the 16 datasets (in four geographical groups). Each dataset is represented by the four panels in a row. Within a panel, each point represents one of 9 or 10 elevations within the (rescaled) domain at which variables were evaluated. *First panel:* the regression of empirical richness *vs.* the modeled midpoint attractor. *Second panel:* unity-line regression (*slope* = 1, Romdal *et al.* 2005) of modeled richness *vs.* empirical richness. *Third panel*: regression of the modeled midpoint attractor *vs.* the best-fitting (by AIC) environmental variables. *Fourth panel:* the regression of empirical species richness *vs.* the best-fitting (by AIC) environmental variables. See Table S3 for statistical results.

***Appendix 2*, Fig. S2**. Costa Rican fern dataset with no attractor (pure geometric

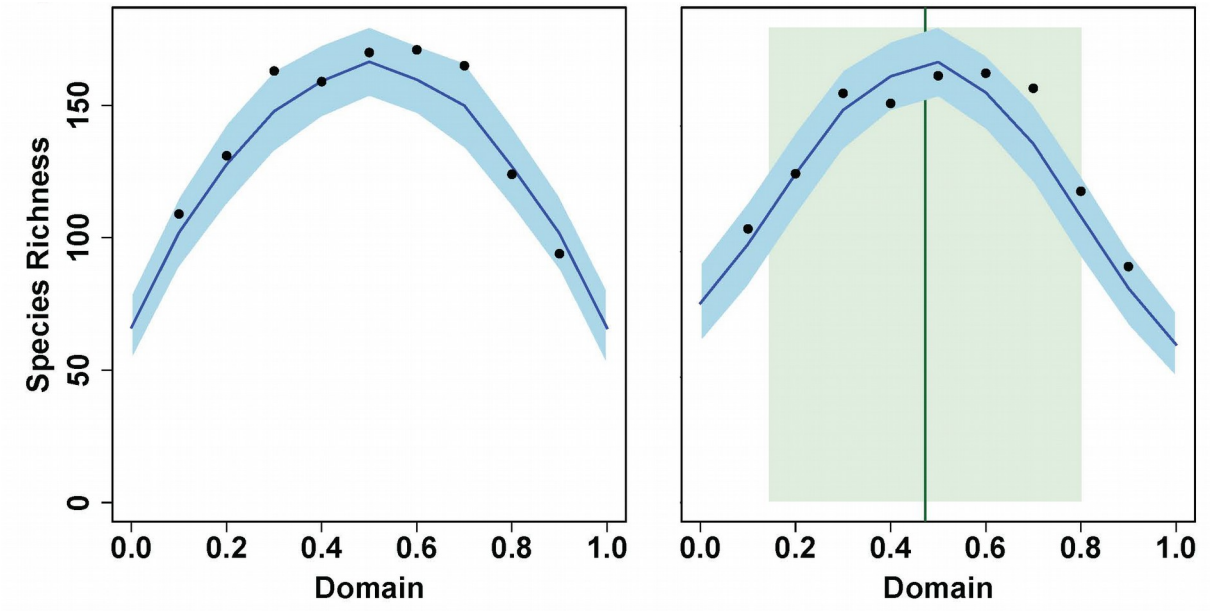

constraints) (*left panel*) and with the best-fit midpoint attractor (*right panel*). The modeled curves differ slightly in shape, but the overall fit is quite similar. Empirical richness values are the black points, identical in the two plots.

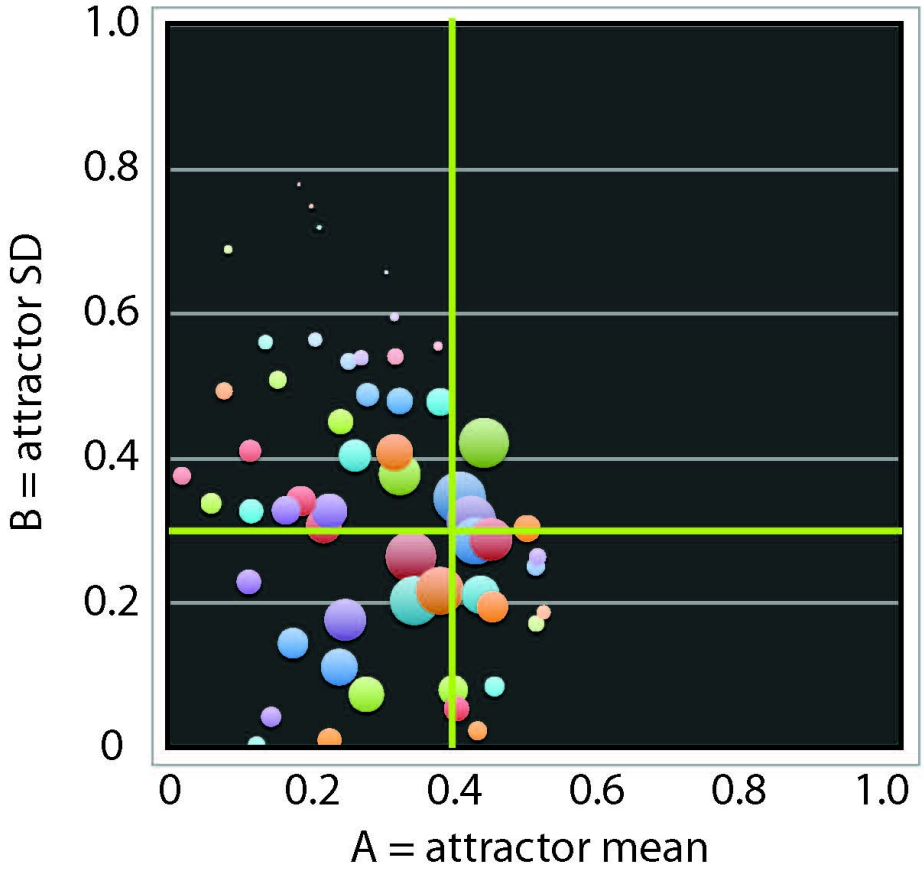

***Appendix 2,* Fig. S3**. Sampled (*A*, *B*) pairs of midpoint attractor parameters generated by the MCMC Gibbs sampler for the Costa Rican arctiine moth dataset. Point width is proportional to the coefficient of determination (R^2) between modeled and observed species richness across the elevational domain. Point color is arbitrary. The green lines indicate the optimized pair of parameter values (A = 0.378, B = 0.294) that yielded the highest R^2, which was used to produce model for the arctiine moth dataset in Fig. 3 (main text).

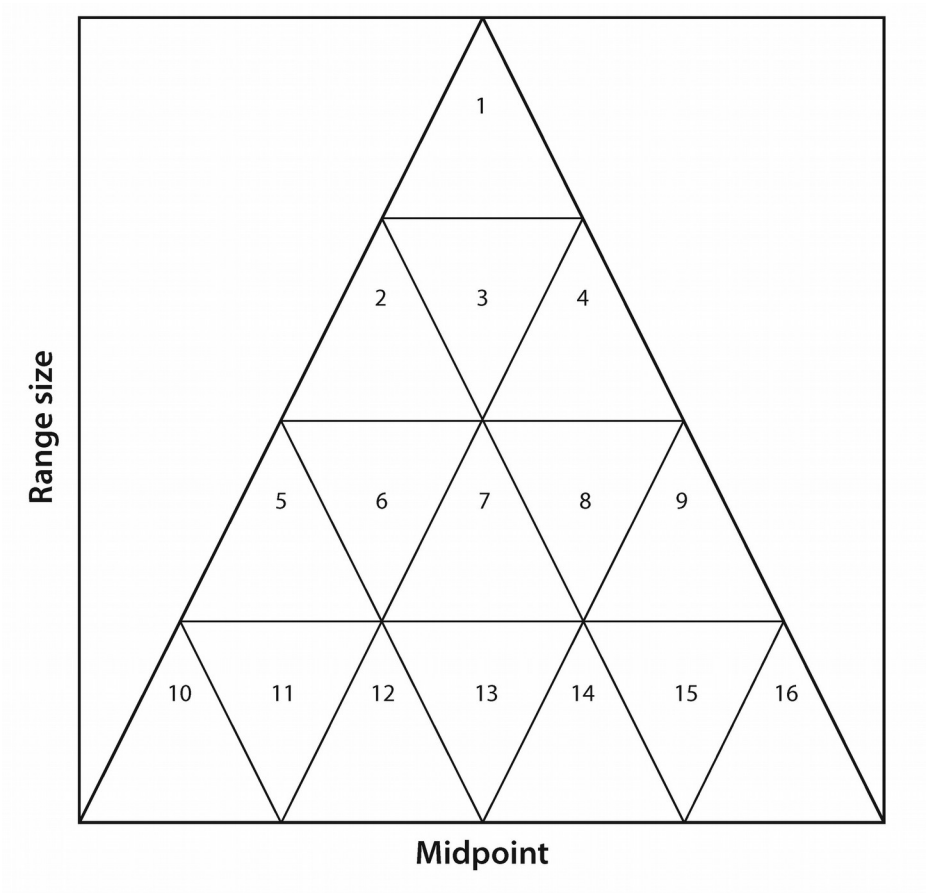

***Appendix 2*, Fig. S4.** The geometric constraint triangle, subdivided into 16 smaller, equal-sized triangles.